NASA Contractor Report 172248

NASA-CR-172248
19840003764

ICASE

SPECTRAL METHODS FOR PARTIAL DIFFERENTIAL EQUATIONS

M. Yousuff Hussaini
Craig L. Streett
Thomas A. Zang

Contract Nos. NAS1-17070, NAS1-17130
August 1983

INSTITUTE FOR COMPUTER APPLICATIONS IN SCIENCE AND ENGINEERING
NASA Langley Research Center, Hampton, Virginia 23665

Operated by the Universities Space Research Association

National Aeronautics and
Space Administration

Langley Research Center
Hampton, Virginia 23665

SPECTRAL METHODS FOR PARTIAL DIFFERENTIAL EQUATIONS

M. Yousuff Hussaini
Institute for Computer Applications in Science and Engineering

Craig L. Streett
NASA Langley Research Center

Thomas A. Zang
NASA Langley Research Center

ABSTRACT

Origins of spectral methods, especially their relation to the Method of Weighted Residuals, are surveyed. Basic Fourier, Chebyshev, and Legendre spectral concepts are reviewed, and demonstrated through application to simple model problems. Both collocation and tau methods are considered. These techniques are then applied to a number of difficult, nonlinear problems of hyperbolic, parabolic, elliptic, and mixed type. Fluid-dynamical applications are emphasized.

Research for the first author was supported by the National Aeronautics and Space Administration under NASA Contract Nos. NAS1-17130 and NASA-17070 while in residence at ICASE, NASA Langley Research Center, Hampton, VA 23665.

INTRODUCTION

Spectral methods may be viewed as an extreme development of the class of discretization schemes known by the generic name of the method of weighted residuals (MWR) [1]. The key elements of the MWR are the trial functions (also called the expansion or approximating functions) and the test functions (also known as weight functions). The trial functions are used as the basis functions for a truncated series expansion of the solution, which, when substituted into the differential equation, produces the residual. The test functions are used to enforce the minimization of the residual.

The choice of trial functions is what distinguishes the spectral methods from the finite element and finite difference methods. The trial functions for spectral methods are infinitely differentiable global functions. (Typically they are tensor products of the eigenfunctions of singular Sturm-Liouville problems.) In the case of finite element methods, the domain is divided into small elements, and a trial function is specified in each element. The trial functions are thus local in character, and well-suited for handling complex geometries. The finite difference trial functions are likewise local.

The choice of test function distinguishes between the Galerkin, collocation, and tau approaches. In the Galerkin approach, the test functions are the same as the trial functions, whereas in the collocation approach the test functions are translated Dirac delta functions. In other words, the Galerkin approach is equivalent to a least squares approximation, whereas the collocation approach requires the differential equation to be satisfied exactly at the collocation points. Spectral tau methods are close to Galerkin methods but they differ in the treatment of boundary conditions.

The collocation approach is the simplest of the MWR, and appears to have been first used by Slater [2] in his study of electronic energy bands in metals. A few years later, Barta [3] applied this method to the problem of the torsion of a square prism. Frazer, et al. [4] developed it as a general method for solving ordinary differential equations. They used a variety of trial functions and an arbitrary distribution of collocation points. The work of Lanczos [5] established for the first time that a proper choice of trial functions and distribution of collocation points is crucial to the accuracy of the solution. Perhaps he should be credited with laying down the foundation of the orthogonal collocation method. This method was revived by Clenshaw [6], Clenshaw and Norton [7], and Wright [8]. These studies involved application of Chebyshev polynomial expansions to initial value problems. Villadsen and Stewart [9] developed this method for boundary value problems.

The earliest investigations of the spectral collocation method to partial differential equations were those of Kreiss and Oliger [10] (who called it the Fourier method) and Orszag [11] (who termed it pseudospectral). This approach is especially attractive because of the ease with which it can be applied to variable coefficient and even nonlinear problems. The essential details will be furnished below.

The Galerkin approach is perhaps the most esthetically pleasing of the MWR since the trial functions and the test functions are the same. Indeed, the first serious application of spectral methods to PDE's -- that of Silberman [12] for meteorological modelling — used the Galerkin approach. However, spectral Galerkin methods only became practical for high resolution calculations of nonlinear problems after Orszag [13] and Eliasen, et al. [14] developed a transform method for evaluating convolution sums arising from quadratic nonlinearities. Even in this case spectral collocation methods

retain a factor of 2 in speed. For more complicated nonlinear terms high resolution spectral Galerkin methods are still impractical.

The tau approach is the most difficult to rationalize within the context of the MWR. Lanczos [5] developed the spectral tau method as a modification of the Galerkin method for problems with non-periodic boundary conditions. Although it too, is difficult to apply to nonlinear problems, it has proven quite useful for constant coefficient problems or subproblems, e.g., for semi-implicit time-stepping algorithms.

The following discussion of spectral methods for PDE's will be organized around the three basic types of systems — hyperbolic, parabolic, and elliptic -- with an additional section for a difficult, nonlinear problem of mixed type. Simple, one-dimensional, linear examples will be provided to illustrate the basic principles and details of the algorithms; two-dimensional, nonlinear examples drawn from fluid dynamical applications will also be furnished to demonstrate the power of the method. The focus will be on collocation methods, although some discussion of tau methods is provided.

II. HYPERBOLIC EQUATIONS

Linear hyperbolic equations are perhaps the simplest setting for describing spectral collocation methods. Both Fourier and Chebyshev schemes have found wide application. This section will first present the fundamentals of both approaches and then illustrate them on a nonlinear fluid dynamics problem involving shock waves.

Basic Fourier Spectral Concepts.

The potential accuracy of spectral methods derives from their use of suitable high-order interpolation formulae for approximating derivatives. An elementary example is provided by the model problem

$$u_t + u_x = 0, \tag{1}$$

with periodic boundary conditions on $[0,2\pi]$ and the initial condition

$$u(x,0) = \sin(\pi \cos x). \tag{2}$$

The exact solution

$$u(x,t) = \sin[\pi \cos(x-t)] \tag{3}$$

has the Fourier expansion

$$u(x,t) = \sum_{k=-\infty}^{\infty} \bar{u}_k(t)\, e^{ikx}, \tag{4}$$

where the Fourier coefficients

$$\bar{u}_k(t) = \sin\left(\frac{k\pi}{2}\right) J_k(\pi)\, e^{-ikt} \tag{5}$$

and $J_k(t)$ is the Bessel function of order k. The asymptotic properties of the Bessel functions imply that

$$k^p\, \bar{u}_k(t) \to 0 \qquad \text{as} \quad k \to \infty \tag{6}$$

for all positive integers p. As a result, the truncated Fourier series

$$u_N(x,t) = \sum_{k=-N/2+1}^{N/2-1} \bar{u}_k(t)\, e^{ikx} \tag{7}$$

converges faster than any finite power of 1/N. This property is often referred to as exponential convergence. A straightforward integration-by-parts argument [15] may be used to show that it applies to any periodic and infinitely differentiable solution.

The standard collocation points are

$$x_j = \frac{2\pi j}{N} \qquad j=0,1,\cdots,N-1. \tag{8}$$

Let u_j denote the approximation to $u(x_j)$, where the time dependence has been suppressed. Then the spatial discretization of Eq. (1) is

$$\frac{\partial u_j}{\partial t} = \frac{\partial \tilde{u}}{\partial x}\Big|_j , \tag{9}$$

where the right-hand-side is determined as follows. First, compute the discrete Fourier coefficients

$$\hat{u}_k = \frac{1}{N} \sum_{j=0}^{N-1} u_j\, e^{-ikx_j}, \qquad k= -\frac{N}{2}, -\frac{N}{2}+1, \cdots, \frac{N}{2}-1. \tag{10}$$

Then the interpolating function

$$\tilde{u}(x) = \sum_{k=-N/2}^{N/2-1} \hat{u}_k\, e^{ikx} \tag{11}$$

can be differentiated analytically to obtain

$$\left.\frac{\partial \tilde{u}}{\partial x}\right|_j = \sum_{k=-N/2+1}^{N/2-1} ik\, \hat{u}_k\, e^{ikx_j}. \tag{12}$$

(The term involving $k = -N/2$ makes a purely imaginary contribution to the sum and hence has been dropped.) Note that each derivative approximation uses all available information about the function values. The sums in Eqs. (10) and (12) can be obtained in $O(N \ln N)$ operations via the Fast Fourier Transform (FFT).

An illustration of the superior accuracy available from the spectral method for this problem is provided in Table I. Shown there are the maximum errors at $t = 1$ for the truncated series and for the spectral collocation method as well as for second-order and fourth-order finite difference methods. The time discretization was the classical fourth-order Runge-Kutta method. In all cases the time-step was chosen so small that the temporal discretization error was negligible. Because the solution is infinitely smooth, the convergence of the spectral method on this problem is more rapid than any finite power of $1/N$. (The error for the $N = 64$ spectral result is

Table I. Maximum Error for a 1-D Periodic Problem

N	Truncated Series	Fourier Spectral	2nd-Order Finite Difference	4th-Order Finite Difference
8	9.87 (-2)	1.62 (-1)	1.11 (0)	9.62 (-1)
16	2.55 (-4)	4.97 (-4)	6.13 (-1)	2.36 (-1)
32	1.05 (-11)	1.03 (-11)	1.99 (-1)	2.67 (-2)
64	6.22 (-13)	9.55 (-12)	5.42 (-2)	1.85 (-3)
128			1.37 (-2)	1.18 (-4)

so small that it is swamped by the round-off error of these single precision CDC Cyber 175 calculations.) In most practical applications the benefit of the spectral method is not the extraordinary accuracy available for large N but rather the small size of N necessary for a moderately accurate solution.

Basic Chebyshev Spectral Concepts

Spectral methods for non-periodic problems can also exhibit exponential convergence. A simple example is again provided by Eq. (1) but now on the interval $[-1,1]$ with initial condition $u(x,0)$ and boundary condition $u(-1,t)$. Since this is not a periodic problem, a spectral method based upon Fourier series in x would exhibit extremely slow convergence. However, rapid convergence as well as efficient algorithms can be attained for spectral methods based upon Chebyshev polynomials. These are defined on $[-1,1]$ by

$$\tau_n(x) = \cos\ (n \cos^{-1} x). \tag{13}$$

The function

$$u(x,t) = \sin\ \alpha\pi(x-t) \tag{14}$$

is one solution to Eq. (1). It has the Chebyshev expansion

$$u(x,t) = \sum_{n=0}^{\infty} \bar{u}_n(t)\ \tau_n(x), \tag{15}$$

where

$$\bar{u}_n(t) = \frac{2}{c_n} \sin\left(\frac{n\pi}{2} - \alpha\pi t\right) J_n(\alpha\pi) \tag{16}$$

with

$$c_n = \begin{cases} 2 & n = 0 \\ 1 & n > 1 \end{cases} . \tag{17}$$

The truncated series

$$u_N(x,t) = \sum_{n=0}^{N} \bar{u}_n(t)\, \tau_n(x) \tag{18}$$

converges at an exponential rate. Note that this result holds whether or not α is an integer. In contrast, the Fourier coefficients of $u(x,t)$ are

$$\bar{u}_k(t) = \frac{i}{2\pi} e^{i\alpha\pi t} \frac{\sin \pi(\alpha+k)}{\alpha+k} - \frac{i}{2\pi} e^{-i\alpha\pi t} \frac{\sin \pi(\alpha-k)}{\alpha-k} . \tag{19}$$

For non-integer α these decay extremely slowly.

The change of variables

$$x = \cos \theta, \tag{20}$$

the definition

$$v(\theta,t) = u(\cos \theta, t), \tag{21}$$

and Eq. (13) reduce Eq. (15) to

$$v(\theta,t) = \sum_{n=0}^{\infty} \bar{u}_n(t) \cos n\theta. \tag{22}$$

Thus, the Chebyshev coefficients of $u(x,t)$ are precisely the Fourier coefficients of $v(\theta,t)$. This new function is automatically periodic. If $u(x,t)$ is infinitely differentiable (in x), then $v(\theta,t)$ will be infinitely differentiable (in θ). Hence, straightforward integration-by-parts arguments lead to the conclusion that the Chebyshev coefficients of an infinitely

differentiable function will decay exponentially fast. Note that this holds regardless of the boundary conditions.

A Chebyshev spectral method makes use of the interpolating function

$$\tilde{u}(x) = \sum_{n=0}^{N} \hat{u}_n \, \tau_n(x). \tag{23}$$

The standard collocation points are

$$x_j = \cos \frac{\pi j}{N} \qquad j = 0,1,\cdots,N. \tag{24}$$

Thus,

$$u_j = \sum_{n=0}^{N} \hat{u}_n \cos \frac{n\pi j}{N} , \tag{25}$$

where u_j is the approximation to $u(x_j)$. The inverse relation is

$$\hat{u}_n = \frac{2}{N\bar{c}_n} \sum_{j=0}^{N} \bar{c}_j^{-1} \, u_j \cos \frac{n\pi j}{N} , \qquad n = 0,1,\cdots,N \tag{26}$$

where

$$\bar{c}_j = \begin{cases} 2 & j = 0 \text{ or } N \\ 1 & 1 \leq j \leq N-1 \end{cases} . \tag{27}$$

The analytic derivative of this function is

$$\frac{\partial \tilde{u}}{\partial x} = \sum_{n=0}^{N} \hat{u}_n^{(1)} \, \tau_n(x), \tag{28}$$

where

$$\hat{u}^{(1)}_{N+1} = 0$$

$$\hat{u}^{(1)}_{N} = 0 \tag{29}$$

$$\bar{c}_n \hat{u}^{(1)}_n = \hat{u}^{(1)}_{n+2} + 2(n+1)\hat{u}_{n+1}, \qquad n = N-1, N-2, \cdots, 0.$$

(See [15] for the derivation of this recursion relation.) The Chebyshev spectral derivatives at the collocation points are

$$\left.\frac{\partial \tilde{u}}{\partial x}\right|_j = \sum_{n=0}^{N} \hat{u}^{(1)}_n \cos\frac{\pi j n}{N} . \tag{30}$$

Special versions of the FFT may be used for evaluating the sums in Eqs. (26) and (30). The total cost for a Chebyshev spectral derivative is thus $O(N \ln N)$.

The time-stepping scheme for Eq. (1) must use the boundary conditions to update u_N (at $x = -1$) and the approximate derivatives from Eq. (30) to update u_j for $j=0,1,\cdots,N-1$. Note that no special formula is required for the derivative at $j = 0$ (or $x = +1$).

Results pertaining to $\alpha = 2.5$ at $t = 1$ for a truncated Chebyshev series, a Chebyshev spectral method, a Fourier spectral method, and a second-order finite difference method are given in Table II. For this non-periodic problem Fourier spectral methods are quite inappropriate, but the Chebyshev spectral method is far superior to the finite difference method.

The Chebyshev collocation points are the extreme points of $T_N(x)$. Note that they are not evenly distributed in x, but rather are clustered near the endpoints. The smallest mesh size scales as $1/N^2$. While this distribution contributes to the quality of the Chebyshev approximation and permits the use

of the FFT in evaluating the series, it also places a severe time-step limitation on explicit methods for evolution equations.

Table II. Maximum Error for a 1-D Dirichlet Problem

N	Truncated Series	Chebyshev Spectral	Fourier Spectral	Finite Difference
4	1.24 (0)	1.49 (0)	1.85 (0)	1.64 (0)
8	1.25 (-1)	6.92 (-1)	1.92 (0)	1.73 (0)
16	7.03 (-6)	1.50 (-4)	2.27 (0)	1.23 (0)
32	1.62 (-13)	3.45 (-11)	2.28 (0)	3.34 (-1)
64	1.79 (-13)	9.55 (-11)	2.27 (0)	8.44 (-2)

Application to Two-dimensional, Supersonic Flow

Spectral methods have recently been applied successfully to the nonlinear hyperbolic system of equations which describes a two-dimensional inviscid gas [16,17]. The most serious complication over the simple model problems discussed above occurs when shock waves are present. If the shock occurs in the interior of the domain, then the truncated series for the discontinuous flow variables converges very slowly. Elaborate filtering strategies appear necessary to extract useful information from a calculation of such a situation [17,18]. This difficulty disappears, however, when the shock occurs at the boundary of the domain, as in shock-fitting as opposed to shock-capturing calculations.

A schematic of the type of spectral shock-fitted calculations described below is illustrated in Fig. 1. At time $t = 0$ an infinite, normal shock

at $x = 0$ separates a rapidly moving, uniform fluid on the left from the fluid on the right which is in a quiescent state except for some specified fluctuation. The initial conditions are chosen so that in the absence of any fluctuation the shock moves uniformly in the positive x-direction with a Mach number (relative to the fluid on the right) denoted by M_s. In the presence of fluctuations the shock front will develop ripples. The shape of the shock is described by the function $x_s(y,t)$. The numerical calculations are used to determine the state of the fluid in the region between the shock front and some suitable left boundary $x_L(t)$ and also to determine the motion and shape of the shock front itself.

Figure 1 is taken from a shock/turbulence calculation [19] in which the downstream fluctuation is a plane vorticity wave that is periodic in y with period y_ℓ. Because of the initial value nature of the calculation, the fluid motion behind the shock is not periodic in x, as Fig. 1 makes abundantly clear. The interesting physical domain is given by

$$x_L(t) \leq x \leq x_s(y,t)$$

$$0 \leq y \leq y_\ell \tag{31}$$

$$t \geq 0.$$

The change of variables

$$X = \frac{x - x_L(t)}{x_s(y,t) - x_L(t)}$$

$$Y = y/y_\ell \tag{32}$$

$$T = t$$

produces the computational domain

$$\begin{cases} 0 < X < 1 \\ 0 < Y < 1 \\ T > 0. \end{cases} \tag{33}$$

The fluid motion is modeled by the two-dimensional Euler equations. In terms of the computational coordinates these are

$$Q_T + B\,Q_X + C\,Q_Y = 0, \tag{34}$$

where $Q = (P,u,v,S)^T$,

$$B = \begin{bmatrix} U & \gamma X_x & \gamma X_y & 0 \\ \frac{a^2}{\gamma} X_x & U & 0 & 0 \\ \frac{a^2}{\gamma} X_y & 0 & U & 0 \\ 0 & 0 & 0 & U \end{bmatrix} \tag{35}$$

and

$$C = \begin{bmatrix} V & \gamma Y_x & \gamma Y_y & 0 \\ \frac{a^2}{\gamma} Y_x & V & 0 & 0 \\ \frac{a^2}{\gamma} Y_y & 0 & V & 0 \\ 0 & 0 & 0 & V \end{bmatrix} . \tag{36}$$

The contravariant velocity components are given by

$$U = X_t + uX_x + vX_y$$

and (37)

$$V = Y_t + uY_x + vY_y .$$

A subscript denotes partial differentiation with respect to the indicated variable. P, a, and S are all normalized by reference conditions at downstream infinity; u and v are velocity components in the x and y directions, both scaled by the characteristic velocity defined by the square root of the pressure-density ratio at downstream infinity. A value $\gamma = 1.4$ has been used.

Let n denote the time level and Δt the time increment. The time discretization of Eq. (34) is

$$\tilde{Q} = [1 - \Delta t L^n] Q^n \tag{38}$$

$$Q^{n+1} = \frac{1}{2} [Q^n + (1 - \Delta t \tilde{L}) \tilde{Q}], \tag{39}$$

where L denotes the spatial discretization of $B\partial_X + C\partial_Y$. The solution Q has the Chebyshev - Fourier series expansion

$$Q(X,Y,T) = \sum_{p=0}^{M} \sum_{q=-N/2}^{N/2-1} Q_{pq}(T)\, \tau_p(\xi) e^{2\pi i q Y}, \tag{40}$$

where $\xi = 2X-1$. The derivatives Q_X and Q_Y are approximated by

$$Q_X = 2 \sum_{p=0}^{M} \sum_{q=-N/2}^{N/2-1} Q^{(1,0)}_{pq}(T) \tau_p(\xi) e^{2\pi i q Y}, \tag{41}$$

$$Q_Y = 2\pi \sum_{p=0}^{M} \sum_{q=-N/2}^{N/2-1} Q^{(0,1)}_{pq}(T) \tau_p(\xi) e^{2\pi i q Y}, \tag{42}$$

where $Q^{(1,0)}_{pq}$ is computed from Q_{pq} in a manner analogous to Eq. (29), and

$$Q^{(0,1)}_{pq} = i\, q\, Q_{pq}. \tag{43}$$

As a general rule the correct numerical boundary conditions for a spectral method are the same as the correct analytical boundary conditions. The global nature of the approximation avoids the need for special differentiation formulae at boundaries. At the same time spectral methods are quite unforgiving of incorrect boundary conditions. The inherent dissipation of these methods is so low that boundary errors quickly contaminate the entire solution. In many fluid dynamical applications the computational region must be terminated at some finite, artificial boundary. The difficulty at "artificial" boundaries is that analytically correct, fully nonlinear boundary conditions for systems are seldom known. One example of a workable artificial boundary condition for the Euler equations is given in Ref. [20].

The most critical part of the calculation is the treatment of the shock front. The shock-fitting approach used here is desirable because it avoids the severe post-shock oscillations that plague shock-capturing methods. The time derivative of the Rankine-Hugoniot relations provides an equation for the

shock acceleration. This equation is integrated to update the shock position (see [20] for details). This method is a generalization of the finite difference method developed by Pao and Salas [21] for their study of the shock/vortex interaction.

The nonlinear interaction of plane waves with shocks was examined at length in [19]. The numerical method used there was similar to the one described above but employed second-order finite differences in place of the present Chebyshev-Fourier spectral discretization. Detailed comparisons were made in [19] with the predictions of linear theory [22]. The linear results turned out to be surprisingly robust, remaining valid at very low (but still supersonic) Mach numbers and at very high incident wave amplitudes. The only substantial disagreement occurred for incident waves whose wave fronts were nearly perpendicular to the shock front. This type of shock-turbulence interaction is a useful test of the spectral technique because the method can be calibrated in the regions for which linear theory has been shown to be valid.

The most reliable numerical results can be obtained for the acoustic responses to acoustic waves. Unlike the vorticity responses, these require no differentiation of the flow variables, thus eliminating one extra source of error. Moreover, the acoustic reponse stretches much further behind the shock than the vorticity response, thus providing greater statistical reliability. Vorticity response results are reported in [23]. The incident pressure wave is taken to be

$$p_1' = A_1' \, e^{i(\underline{k}_1 \cdot \underline{x} - \omega_1 t)} \tag{44}$$

where $\underline{k}_1 = (k_{1,x}, k_{1,y})'$, $\omega = M_s a_1 k_{1,x} + a_1 k_1$ and A_1' is the amplitude. In

terms of the incidence angle θ_1, $\underline{k}_1 = (k_1 \cos\theta_1, k_1 \sin\theta_1)$. The linearized transmitted acoustic wave can be expressed in the same manner with all subscripts changed from 1 to 2. The amplification coefficient for the transmitted acoustic wave is then the ratio

$$\tilde{A_2}/\tilde{A_1} \ . \tag{45}$$

Figure 2 indicates the transmission coefficient extracted from the computation. At each fixed value of X we perform a Fourier analysis in Y of the pressure. The Fourier coefficient for $q = 1$ provides the amplitude $\tilde{A_2}$. In order to reduce the transients that would accompany an abrupt start of the calculation at full wave amplitude, an extra factor of $s(t)$ is inserted into Eq. (44), where

$$s(t) = \begin{cases} 3(t/t_s)^2 - 2(t/t_s)^3 & 0 \leq t \leq t_s \\ 1 & t > t_s \end{cases} \ . \tag{46}$$

The start-up time t_s is some multiple (typically $1/2$) of the time it takes the shock to encounter one full wavelength (in the x-direction) of the incident wave. The ratio $\tilde{A_2}/\tilde{A_1}$ is plotted in Fig. 2 as a function of the mean value of the physical coordinate x corresponding to X. The start-up time for this Mach 3 case is $t_s = 0.56$. The average of the x-dependent responses between the start-up interval and the shock produces the computed transmission coefficient. The standard deviation of the individual responses serves as an error estimate.

The dependence upon incidence angle of the acoustic transmission coefficient for $\tilde{A_1} = 0.001$ and $M_s = 3$ waves is displayed in Fig. 3. As is discussed in [19], linear theory is quite reliable at angles below, say,

45°. Figure 3 contains results from both spectral and finite difference calculations. The finite difference results were obtained with the same second-order MacCormack's method that was described in [19] except that periodic boundary conditions (rather than stretching) were employed in the y-direction. The finite difference grid was 64 × 16 and these calculations used a CFL number of 0.70. The spectral grid was 32 × 8, and the CFL number was 0.50. Figure 3 shows that both methods produce the same results. A head-to-head comparison of both methods for the $\theta_1 = 10^\circ$ case is provided in Table III. The "exact" value is taken from linear theory [22]. Since the amplitude of the incident acoustic wave is so small, it should come as no surprise that four points in the y-direction suffice for the spectral calculation. Note that the standard deviations are substantially smaller for the spectral method. These results suggest that the spectral method requires only half as many grid points in each coordinate direction.

Table III. Grid Dependence of Acoustic Transmission Coefficient

Grid	Finite Difference	Chebyshev-Fourier Spectral
16 × 4	6.403 ± 2.652	7.257 ± 0.587
16 × 8	6.427 ± 2.626	7.257 ± 0.587
32 × 4	7.105 ± 0.453	7.158 ± 0.022
32 × 8	7.134 ± 0.471	7.158 ± 0.022
32 × 16	7.139 ± 0.497	7.158 ± 0.022
64 × 16	7.163 ± 0.078	7.157 ± 0.017
128 × 16	7.152 ± 0.022	
"exact"	7.156	7.156

III. PARABOLIC EQUATIONS

The nonlinear, parabolic system formed by the incompressible, Navier-Stokes equations was the focus of much of the early development and application of spectral methods to large-scale fluid dynamical problems. Fourier spectral methods have been the obvious choice for the simulation of homogeneous, isotropic turbulence [24]. For shear flows, however, non-periodic boundary conditions are required. So far, Chebyshev spectral methods have been favored for these applications [25-27]. Nevertheless, Legendre spectral methods are a viable alternative and of late they have been attracting some attention. This section will present a discussion of the implementation of Legendre spectral methods and will then compare them with Chebyshev spectral methods for the one-dimensional heat equation. This section will close with a description of a promising semi-implicit time-stepping scheme for the Navier-Stokes equations.

Basic Legendre Spectral Concepts

A Legendre spectral method on $[-1,1]$ makes uses of the interpolating function

$$\tilde{u}(x) = \sum_{n=0}^{N} \hat{u}_n P_n(x), \tag{47}$$

where $P_n(x)$ is the Legendre polynomial of degree n. Closed form expressions for these polynomials are well-known, albeit clumsy. The computationally preferred way to evaluate the polynomials is through the recursion relation

$$P_0(x) = 1$$

$$P_1(x) = x$$

and for $n \geq 2$

$$n\, P_n(x) = (2n-1)xP_{n-1}(x) - (n-1)\, P_{n-2}(x). \tag{48}$$

Unlike the case with Fourier and Chebyshev collocation methods, there is no tidy expression for the Legendre collocation points. Appeal must be made to the theory of numerical quadrature [28]. The presence of boundary conditions at both endpoints makes it desirable to include -1 and +1 in the set of collocation points. Subject to this constraint, the most accurate quadrature formula for the discrete Legendre coefficients is the Gauss-Lobatto rule

$$\hat{u}_n = \hat{c}_n \sum_{j=0}^{N} w_j \, P_n(x_j) \, u_j, \qquad n = 0,1,\cdots,N \tag{49}$$

where $x_0 = +1$, $x_N = -1$ and x_j for $1 \leq j \leq N-1$ are the roots of $P_N'(x)$. The weights are

$$w_j = \frac{1}{N(N+1) \, P_N^2(x_j)}, \tag{50}$$

and

$$\hat{c}_n = \begin{cases} 2n+1 & n = 0,1,\cdots,N-1 \\ N & n = N \end{cases}. \tag{51}$$

The interior collocation points must be determined numerically. This quadrature rule yields the exact Legendre coefficients if $u(x)$ is any polynomial of degree less than N. Its inverse relation is

$$u_j = \sum_{n=0}^{N} \hat{u}_n \, P_n(x_j). \tag{52}$$

The analytic derivative of the interpolating function in Eq. (47) is

$$\frac{\partial \tilde{u}}{\partial x} = \sum_{n=0}^{N} \hat{u}_n^{(1)} P_n(x), \tag{53}$$

where

$$\hat{u}_{N+1}^{(1)} = 0$$

$$\hat{u}_N^{(1)} = 0 \tag{54}$$

$$\frac{1}{2n+1} \hat{u}_n^{(1)} = \frac{1}{2n+5} \hat{u}_{n+2}^{(1)} + \hat{u}_{n+1} \qquad n = N-1, N-2, \cdots, 0.$$

Since fast transform techniques are not available for the Legendre basis functions, there is no particular advantage to computing $\partial \tilde{u}/\partial x|_j$ by applying Eqs. (49), (54) and (53) rather than by following Eq. (49) with

$$\frac{\partial \tilde{u}}{\partial x}\Big|_j = \sum_{n=0}^{N} \hat{u}_n P_n'(x_j). \tag{55}$$

In fact, for a collocation method it is faster still to perform this entire process by a single matrix-vector multiplication. For that matter the Chebyshev collocation differentiation operator may also be represented by a matrix. Timing studies [29] on the CDC Cyber 175 have indicated that even for $N = 16$, the Chebyshev matrix-multiply differentiation procedure is substantially faster than one based on assembly language fast transforms. Moreover, the matrix-multiply procedure does not suffer the sort of speed degradation that afflicts the transform procedure whenever N is not an integral power of 2.

The heat equation

$$\frac{\partial u}{\partial t} = \frac{\partial^2 u}{\partial x^2} \tag{56}$$

is the natural parabolic linear model problem. The spatial domain is $[-1,1]$, the initial condition is

$$u(x,0) = \sin \pi x \tag{57}$$

and the boundary conditions are

$$\begin{aligned} u(-1,t) &= 0 \\ u(+1,t) &= 0. \end{aligned} \tag{58}$$

The exact solution is then

$$u(x,0) = e^{-\pi^2 t} \sin \pi x. \tag{59}$$

The time differencing is again the classical fourth-order Runge-Kutta scheme.

In addition to spectral collocation and series truncation solutions, we will also present spectral tau results. Let $\bar{u}_n(t)$ for $n=0,1,\cdots,N$ denote the Legendre coefficients of the tau approximation to $u(x,t)$. The semi-discrete tau equations are

$$\frac{d\bar{u}_n}{dt} = \bar{u}_n^{(2)}, \qquad n = 0,1,\cdots,N-2 \tag{60}$$

with

$$\begin{aligned} \sum_{\substack{n=0 \\ n \text{ even}}}^{N} \bar{u}_n &= 0 \\ \sum_{\substack{n=1 \\ n \text{ odd}}}^{N} \bar{u}_n &= 0. \end{aligned} \tag{61}$$

The Legendre coefficients of the approximation to the second spatial derivative $\overline{u}_n^{(2)}(t)$ can be obtained from $\overline{u}_n(t)$ by two applications of the recursion relation in Eq. (54). In this tau approximation the dynamical equations for the two highest-order coefficients are dropped in favor of the equations for the boundary conditions. Equation (61) follows from the property

$$P_n(\pm 1) = (\pm 1)^n. \tag{62}$$

Since the Chebyshev polynomials also satisfy Eq. (62), the Chebyshev tau equations for Eq. (56) are the same as Eqs. (60) and (61). Of course, Eq. (29) is invoked for the derivative coefficients instead of Eq. (54).

The results at $t = 1$ are given in Tables IV and V. The maximum errors shown there have been boosted up by the factor e^{π^2} so that they represent relative errors. On the whole the collocation results are the best. Moreover, except for the truncated series results, the Legendre approximations are superior to the Chebyshev ones. Lanczos [30] has discussed some circumstances under which Legendre approximations are superior to Chebyshev ones. It goes almost without saying that finite difference results are far inferior to any of these spectral approximations.

Table IV. Maximum Error for Legendre Approximations to the Heat Equation

N	Truncated Series	Tau	Collocation
8	6.65 (-4)	6.85 (-4)	2.40 (-5)
10	1.72 (-5)	1.07 (-5)	1.50 (-7)
12	3.06 (-7)	1.54 (-7)	1.38 (-9)
14	3.50 (-9)	1.86 (-9)	4.81 (-10)
16	3.88 (-11)	1.15 (-10)	9.98 (-11)

Table V. Maximum Error for Chebyshev Approximations to the Heat Equation

N	Truncated Series	Tau	Collocation
8	2.44 (-4)	1.61 (-3)	4.58 (-4)
10	5.76 (-6)	2.12 (-5)	8.25 (-6)
12	9.42 (-8)	3.19 (-7)	1.01 (-7)
14	1.14 (-9)	3.35 (-9)	1.10 (-9)
16	1.05 (-11)	8.39 (-11)	2.09 (-11)

The time-step restriction for explicit Legendre or Chebyshev methods for the heat equation is very severe, scaling as $1/N^4$. This can pose quite a barrier to large-scale calculations for which a relative accuracy of 0.1% or so will suffice. Fortunately, many large-scale calculations can be split into one-dimensional, inhomogeneous counterparts of Eq. (56) and efficient implicit schemes are available for this linear, constant coefficient equation. They rely on reducing the Legendre (or Chebyshev) tau equations to a system which

is nearly tridiagonal. The Legendre tau equations for a Crank-Nicolson temporal discretization of Eq. (56) are

$$\frac{\lambda}{(2n-1)(2n-3)}\,\bar{u}_{n-2} + \left[1 - \frac{2\lambda e_{n+2}}{(2n-1)(2n+3)}\right]\bar{u}_n + \frac{\lambda e_{n+4}}{(2n+3)(2n+5)}\,\bar{u}_{n+2}$$

$$= \frac{1}{(2n-1)(2n-3)}\,\bar{f}_{n-2} - \frac{2e_{n+2}}{(2n-1)(2n+3)}\,\bar{f}_n + \frac{e_{n+4}}{(2n+3)(2n+5)}\,\bar{f}_{n+2}$$

$$n = 2,3,\cdots,N, \qquad (63)$$

where $\lambda = -\Delta t/2$ with Δt the time-step, the coefficients $\bar{u}_n$ on the left-hand side are at $t + \Delta t$,

$$\bar{f}_n = \bar{u}_n(t) + \frac{1}{2}\,\Delta t\,\bar{u}_n^{(2)}(t), \qquad (64)$$

and

$$e_n = \begin{cases} 1 & 0 \leq n \leq N \\ 0 & n > N \end{cases} . \qquad (65)$$

Equation (63) for even n plus the first of Eqs. (61) form a linear system which is tridiagonal except for the boundary condition equation. This is cheap to invert. The odd coefficients display a similar structure. The Chebyshev tau version of Eq. (63) is available in [15] and [31].

Application to Channel Flow

Several three-dimensional Navier-Stokes algorithms have been developed which incorporate the quasi-tridiagonal structure of the Chebyshev tau equations for the second derivative in semi-implicit schemes which treat the

constant coefficient diffusion term implicitly [25-27]. In practice this device has permitted time-steps several orders of magnitude larger than the explicit diffusion limit. Unfortunately, the quasi-tridiagonal structure is lost even for a linear, variable viscosity coefficient. An effective iterative scheme for this more general case has recently been proposed[1]. This approach will be described here in its two-dimensional setting.

The rotation form equations for two-dimensional channel flow are

$$u_t - v(v_x - u_y) + P_x = (\mu u_x)_x + (\mu u_y)_y$$

$$v_t + u(v_x - u_y) + P_y = (\mu v_x)_x + (\mu v_y)_y \qquad (66)$$

$$u_x + v_y = 0,$$

with periodic boundary conditions in x and no-slip boundary conditions at $y = \pm 1$. The variable P denotes the total pressure. The viscosity μ is presumed to depend upon y.

A useful discretization employs Fourier series in x and Chebyshev series in y. The pressure gradient term and the incompressibility constraint are best handled implicitly. So, too, are the vertical diffusion terms because of the fine mesh-spacing near the wall. The variable viscosity prevents the standard Poisson equation for the pressure from decoupling from the velocities in the diffusion term. The algorithm described in [26] appears

---

[1]Malik, M. R., High Technology Corp., Hampton, VA; Zang, T. A., College of William and Mary, Williamsburg, VA and Hussaini, M. Y., ICASE, NASA Langley Research Center, Hampton, VA., 1982, in preparation.

to be a good starting point. A Crank-Nicolson approach is used for the implicit terms and Adams-Bashforth for the remainder. After a Fourier transform in x, the equations for each wavenumber k have the following implicit structure

$$\hat{u} - \tfrac{1}{2}\Delta t(\mu\hat{u}_y)_y + \tfrac{1}{2}\Delta t ik\hat{P} = \cdots$$

$$\hat{v} - \tfrac{1}{2}\Delta t(\mu\hat{v}_y)_y + \tfrac{1}{2}\Delta t\hat{P}_y = \cdots \qquad (67)$$

$$ik\hat{u} + \hat{v}_y = 0.$$

Fourier transformed variables are denoted by hats, the subscript y denotes a Chebyshev spectral derivative, and Δt is the time increment.

The algorithm in [26] was devised for constant viscosity, in which case the Eqs. (67) can be reduced to essentially a block-tridiagonal form. This cannot be done in the present, more general situation. We advocate solving these equations iteratively after applying a finite difference pre-conditioning.

The interesting physical problems have high Reynolds number, i.e., low viscosity. Thus the first derivative terms in Eqs. (67) predominate. The effective pre-conditioning of them is crucial. Four possibilities have been considered. The eigenvalues of pre-conditioned iterations for the model scalar problem $u_x = f$ with periodic boundary conditions on $[0,2\pi]$ are given for each possibility in Table VI. The term $\alpha\Delta x$ is the product of a wavenumber α and the grid spacing Δx. It falls in the range $0 \leq |\alpha\Delta x| \leq \pi$. For the staggered grid case the discrete Eqs. (67) are modified so that the velocities and the momentum equations are defined at the cell faces $y_j = \cos(\pi j/N)$, $j=0,1,\cdots,N$, whereas the pressure and the

continuity equation are defined at the cell centers $y_{j-1/2} = \cos(\pi(j-1/2)/N)$, $j=1,\cdots,N$. Fast cosine transforms enable interpolation between cell faces and cell centers to be implemented efficiently. The staggered grid for the Navier-Stokes equations has the advantage that no artificial boundary condition is required for the pressure at the walls.

The actual eigenvalues for pre-conditioned iterations of Eqs. (67) are displayed in Fig. 4. The model problem estimates the eigenvalue trends surprisingly well considering that it is just a scalar equation, has only first derivative terms and uses Fourier series rather than Chebyshev polynomials.

The preceding results indicate that the staggered grid leads to the most effective treatment of the first derivative terms. The condition number of the pre-conditioned system is reasonably small and no resolution is lost by a high mode cut-off. (Although it is possible to devise a high-mode cut-off which avoids the small eigenvalues shown in the figures, some of the spectral resolution is thereby lost.) A simple and effective iterative scheme for this system with its complex eigenvalues is a minimum residual method. At a Reynolds number of 7500 each iteration reduces the residual by almost an order of magnitude.

Table VII presents a comparison of the accuracy of the Chebyshev discretization in y. The two codes are otherwise identical. The initial condition consisted of Poiseuille flow plus a small amount of a linearly unstable eigenmode. The table compares the computed growth rate of this perturbation with the theoretical, linear result after 100 time-steps.

Table VI. Pre-conditioned Eigenvalues for a One-dimensional First Derivative Model Problem

PRE-CONDITIONING	EIGENVALUES
Central Differences	$\frac{\alpha\Delta x}{\sin(\alpha\Delta x)}$
One-sided Differences	$e^{-i(\alpha\Delta x/2)} \frac{\alpha\Delta x/2}{\sin[(\alpha\Delta x)/2)]}$
High Mode Cut-off	$\begin{cases} \frac{\alpha\Delta x}{\sin(\alpha\Delta x)} & 0 \leq \lvert\alpha\Delta x\rvert \leq (2\pi/3) \\ 0 & (2\pi/3) < \lvert\alpha\Delta x\rvert \leq \pi \end{cases}$
Staggered Grid	$\frac{(\alpha\Delta x)/2}{\sin[(\alpha\Delta x)/2]}$

Table VII. Percent Error in Growth Rate

N	Finite Difference	Spectral
8	4470	3210
16	337	74.5
32	147	0.097
64	39.5	0.071
128	10.0	
256	2.4	

IV. ELLIPTIC EQUATIONS

Fruitful nonlinear applications of spectral methods developed the latest for equations of elliptic type. Unlike hyperbolic or parabolic equations, for which explicit schemes can often be tolerated, ellipic equations virtually require implicit iterative schemes in practical situations. It was only a few years ago that Morchoisne [32] and Orszag [33] proposed preconditioning the spectral collocation equations by finite difference operators. More recently still, effective spectral multigrid iterative methods have been developed [34,35] and applied to the nonlinear potential flow problem of fluid dynamics [29]. These developments will be described in this section.

Poisson's Equation

As usual the discussion will begin with a linear model problem, but this time in two spatial dimensions. That problem is the Poisson's equation

$$\frac{\partial^2 u}{\partial x^2} + \frac{\partial^2 u}{\partial y^2} = f \tag{68}$$

on the square $[-1,1] \times [-1,1]$ with homogeneous Dirichlet boundary conditions. The choice

$$f(x,y) = -2\pi^2 \sin \pi x \sin \pi y \tag{69}$$

corresponds to the analytical solution

$$u(x,y) = \sin \pi x \sin \pi y. \tag{70}$$

Both Chebyshev and Legendre spectral methods are appropriate for this problem. Direct solution schemes for the Chebyshev tau method have been

described in [31]. The same schemes also work for the Legendre tau method with straightforward modifications. They are basically of an alternating direction implicit (ADI) nature and rely on the quasi-tridiagonal form of the constant coefficient, one-dimensional problem. Haidvogel and Zang [31] report comparisons of the Chebyshev tau method with finite difference methods on numerous problems. They discuss both computational efficiency and accuracy.

These direct solution schemes cannot feasibly be extended to spectral collocation methods because the collocation equations for the one-dimensional components cannot be represented by sparse matrices. However, an ADI iterative scheme based on finite difference preconditioning is an efficient method for obtaining an approximate solution. The description of this scheme in its general nonlinear setting begins by writing the spectral collocation equations as

$$M(U) = 0. \tag{71}$$

Define the Jacobian

$$J(U) = \frac{\partial M}{\partial U}(U). \tag{72}$$

In many cases the Jacobian can be split into the sum of two operators $J_x(U)$ and $J_y(U)$, each involving derivatives in only the one coordinate direction indicated by the subscript. The most straightforward ADI method is

$$[\alpha I - J_x(V)][\alpha I - J_y(V)]\Delta V = \alpha M(V), \tag{73}$$

with the approximate solution V updated by

$$V \leftarrow V + \omega \Delta V. \tag{74}$$

This is just the Douglas-Gunn version of ADI [36]. The term approximate factorization is commonly used for this type of scheme for the nonlinear potential flow problem [37]. This particular scheme is referred to as AF1. For second-order spatial discretizations the term $[\alpha I - J_x(V)]$ leads to a set of tridiagonal systems, one for each value of y. The second left-hand side factor produces another set of tridiagonal systems. For spectral discretizations, however, these systems are full; hence, Eq. (73) is still relatively expensive to invert. A compromise is to replace J_x and J_y with their second-order finite difference analogs, denoted by H_x and H_y, respectively:

$$[\alpha I - H_x(V)][\alpha I - H_y(V)]\Delta V = \alpha M(V). \tag{75}$$

The spectral approximate factorization scheme consists of Eqs. (74) and (75). The choice of the iteration parameters is discussed in [29].

Table VIII. Maximum Error for Chebyshev Approximations to Poisson's Equation

N	Truncated Series	Tau	Collocation
8	2.88 (-4)	2.79 (-3)	1.17 (-4)
10	6.79 (-6)	5.26 (-5)	2.33 (-6)
12	1.09 (-7)	8.86 (-7)	3.12 (-8)
14	1.34 (-9)	1.09 (-8)	3.27 (-10)
16	1.19 (-11)	9.15 (-11)	2.73 (-12)

The results for the simple model problem are presented in Tables VIII and IX. The trends are the same as they were for the heat equation: the collocation method is more accurate than tau and Legendre polynomials are more accurate than Chebyshev. (Since it is not practical to design a spectral method for PDE's using truncated series, those results have been ignored in this comparison.)

Table IX. Maximum Error for Legendre Approximations to Poisson's Equation

N	Truncated Series	Tau	Collocation
8	6.04 (-4)	1.55 (-3)	1.77 (-5)
10	1.69 (-5)	3.40 (-5)	2.48 (-7)
12	3.05 (-7)	6.05 (-7)	2.27 (-9)
14	3.82 (-9)	6.98 (-9)	1.99 (-11)
16	3.85 (-11)	6.37 (-11)	3.06 (-10)

Spectral Multigrid Methods

Iterative schemes for spectral collocation equations, such as AF1, can be accelerated dramatically by applying multigrid concepts. This technique has been extensively developed for finite difference and finite element discretizations [39] and has recently been applied to spectral discretizations [34,35,29]. Briefly put, multigrid methods take advantage of a property shared by a wide variety of relaxation schemes - potential efficient reduction of the high-frequency error components but unavoidable slow reduction of the low-frequency components.

The fundamentals of spectral multigrid are perhaps easiest to grasp for the simple model problem

$$-\frac{d^2u}{dx^2} = f \tag{76}$$

on $[0,2\pi]$ with periodic boundary conditions. The Fourier approximation to the left-hand side of Eq. (76) at the collocation points is

$$\sum_{p=-N/2+1}^{N/2-1} p^2 \hat{u}_p e^{ipx_j} . \tag{77}$$

The spectral approximation to Eq. (76) may be expressed as

$$LU = F, \tag{78}$$

where

$$U = (u_0, u_1, \cdots, u_{N-1}), \tag{79}$$

$$F = (f_0, f_1, \cdots, f_{N-1}), \tag{80}$$

and L represents the Fourier spectral approximation to $-d^2/dx^2$.

A Richardson's iterative scheme for solving Eq. (78) is

$$V \leftarrow V + \omega(F - LV), \tag{81}$$

where ω is a relaxation parameter. On the right side of the replacement symbol ($\leftarrow$) V represents the current approximation to U, and on the left it represents the updated approximation. The eigenfunctions of L are

$$\xi_j(p) = e^{2\pi ijp/N}, \tag{82}$$

with the corresponding eigenvalues

$$\lambda(p) = p^2, \tag{83}$$

where $j = 0,1,\cdots,N-1$ and $p = -N/2+1,\cdots,N/2-1$. The index p has a natural interpretation as the frequency of the eigenfunction.

The error at any stage of the iterative process is $V - U$; it can be resolved into an expansion in the eigenvectors of L. Each iteration reduces the p'th error component to $\nu(\lambda_p)$ times its previous value, where

$$\nu(\lambda) = 1 - \omega\lambda. \tag{84}$$

The optimal choice of ω results from minimizing $|\nu(\lambda)|$ for $\lambda \in [\lambda_{min},\lambda_{max}]$, where λ_{min} 1 and $\lambda_{max} = N^2/4$. (One need not worry about the $p = 0$ eigenfunction since it corresponds to the mean level of the solution, which is at one's disposal for this problem.) The optimal relaxation parameter for this single-grid procedure is

$$\omega_{SG} = \frac{2}{\lambda_{max} + \lambda_{min}}. \tag{85}$$

It produces the spectral radius

$$\rho_{SG} = \frac{\lambda_{max} - \lambda_{min}}{\lambda_{max} + \lambda_{min}}. \tag{86}$$

Unfortunately, $\rho_{SG} \simeq 1 - 8/N^2$, which implies that $O(N^2)$ iterations are required to achieve convergence.

This slow convergence is the outcome of balancing the damping of the lowest-frequency eigenfunction with that of the highest-frequency one in the minimax problem described after Eq. (84). The multigrid approach takes advantage of the fact that the low-frequency modes ($|p| < N/4$) can be represented just as well on coarser grids. It settles for balancing the middle-frequency eigenfunction ($|p| = N/4$) with the highest-frequency one ($|p| = N/2$), and hence damps effectively only those modes which cannot be resolved on coarser grids. In Eqs. (85) and (86), λ_{min} is replaced with $\lambda_{mid} = \lambda(N/4)$. The optimal relaxation parameter in this context is

$$\omega_{MG} = \frac{2}{\lambda_{max} + \lambda_{mid}} . \tag{87}$$

The multigrid smoothing factor

$$\mu_{MG} = \frac{\lambda_{max} - \lambda_{mid}}{\lambda_{max} + \lambda_{mid}} \tag{88}$$

measures the damping rate of the high-frequency modes. In this example $\mu_{MG} = 0.60$, independent of N. The price of this effective damping of the high-frequency errors is that the low-frequency errors are hardly damped at all. Table X compares the single-grid and multigrid damping factors for $N = 64$. However, on a grid with $N/2$ collocation points, the modes for $|p| \in [N/8, N/4]$ are now the high-frequency ones. They get damped on this grid. Still coarser grids can be used until relaxations are so cheap that one can afford to damp all the remaining modes, or even to solve the discrete equations exactly. For the case illustrated in Table X the high-frequency

error reduction in the multigrid context is roughly 250 times as fast as the single-grid reduction for $N = 64$.

Let us consider just the interplay between two grids. A general, nonlinear fine-grid problem can be written

$$L^f(U^f) = F^f. \tag{89}$$

The shift to the coarse grid occurs after the fine-grid approximation V^f has been sufficiently smoothed by the relaxation process, i.e., after the high-frequency content of the error $V^f - U^f$ has been sufficiently reduced. The related coarse-grid problem is

$$L^c(U^c) = F^c, \tag{90}$$

where

$$F^c = R\left[F^f - L^f(V^f)\right] + L^c(RV^f). \tag{91}$$

The restriction operator R interpolates a function from the fine grid to the coarse grid. The coarse-grid operator and solution are denoted by L^c and U^c, respectively. After an adequate approximation V^c to the coarse-grid problem has been obtained, the fine-grid approximation is corrected via

$$V^f \leftarrow V^f + P(V^c - RV^f). \tag{92}$$

The prolongation operator P interpolates a function from the coarse grid to the fine grid.

A complete multigrid algorithm requires specific choices of the interpolation operators, the coarse-grid operators, and the relaxation schemes. These issues are discussed at length in [34,35,29] for both Fourier and Chebyshev multigrid methods. Numerous linear, variable coefficient examples are also provided there. The more interesting nonlinear examples from [29] are the subject of the remainder of this paper.

Table X. Damping Factors for N = 64

p	Single-Grid	Multigrid
1	.9980	.9984
2	.9922	.9938
4	.9688	.9750
8	.8751	.9000
12	.7190	.7750
16	.5005	.6000
20	.2195	.3750
24	.1239	.1000
28	.5298	.2250
32	.9980	.6000

Application to Two-Dimensional Potential Flow

Until the recent work of Streett [38], the discretization procedures for the potential equation were invariably based on low-order finite difference or finite element methods. Streett used a spectral discretization of the full potential equation and obtained its solution by a single-grid iterative technique. The application of spectral multigrid techniques by Streett, et al.

[29] produced a dramatic acceleration of the iterative scheme. Even in its relatively primitive state the spectral multigrid scheme is competitive, and in some cases unequivocally more efficient, than standard finite difference schemes.

After a conformal mapping from the surface of an airfoil to a circle the potential equation becomes

$$\frac{\partial}{\partial R}\left(R\rho \frac{\partial G}{\partial R}\right) + \frac{\partial}{\partial \Theta}\left(\frac{\rho}{R} \frac{\partial G}{\partial \Theta}\right) = 0, \tag{93}$$

where G is the reduced potential, R and Θ are the computational polar coordinates, and ρ is the fluid density. The reduced potential is periodic in Θ and it satisfies

$$\frac{\partial G}{\partial R} = 0 \qquad \text{at} \quad R = 1, \tag{94}$$

$$G \to 0 \qquad \text{as} \quad R \to \infty, \tag{95}$$

and the Kutta condition. The density is given by the isentropic relation

$$\rho = \left[1 - \frac{\gamma-1}{2} M_\infty^2 (q_r^2 + q_\theta^2 - 1)\right]^{\frac{1}{\gamma-1}}; \tag{96}$$

the ratio of specific heats is denoted by γ, and M_∞ is the Mach number at infinity. The velocity components in the physical (r,θ) plane are

$$\begin{aligned} q_r &= \frac{1}{H} \frac{\partial \Phi}{\partial R} \\ q_\theta &= \frac{1}{RH} \frac{\partial \Phi}{\partial \Theta}, \end{aligned} \tag{97}$$

and the Jacobian between the complex physical plane $(z = re^{i\theta})$ and the complex computational plane $(\sigma = Re^{i\Theta})$ is

$$H = \left|\frac{dz}{d\sigma}\right|. \tag{98}$$

Further details are provided in [38].

The spectral method employs a Fourier series representation in Θ. Constant grid spacing in Θ corresponds to a convenient dense spacing in the physical plane at the leading and trailing edges. The domain in R (with a large, but finite outer cutoff) is mapped onto the standard Chebyshev domain $[-1,1]$ by an analytical stretching transformation that clusters the collocation points near the airfoil surface. The stretching is so severe that the ratio of the largest-to-smallest radial intervals is typically greater than 1000.

The flow past an NACA 0012 airfoil at 4° angle of attack and a freestream Mach number of 0.5 is a challenging subsonic and thus elliptic case. Nevertheless, the spectral solution on a relatively coarse grid captures all the essential details of the flow. The surface pressure coefficient from the spectral code MGAFSP [29] using 16 points in the radial (R) direction, and 32 points in the azimuthal (Θ) direction is displayed in Fig. 5. The symbols denote the solution at the collocation points. For comparison, the result from the finite difference, multigrid, approximate factorization code FL036 [40] is shown as a solid line. The grid used in the benchmark finite difference calculation is so fine (64 × 384 points) that the truncation error is well below plotting accuracy. The FL036 and MGAFSP results are identical to plotting accuracy. The spectral computation on this mesh yields a lift coefficient with truncation error less than 10^{-4}. Spectral solutions on a

16 × 32 grid are thus of more than adequate resolution and accuracy for subsonic flows.

In Fig. 6 are shown convergence histories from FL036, MGAFSP, and the finite difference, approximate factorization, single-grid code TAIR [41]. Meshes which yield approximately equivalent accuracy were chosen. The surface pressure results are the same to plotting accuracy, the lift coefficient is converged in the third decimal place, and the predicted drag coefficient is less than .001. (Actually, the spectral result is an order of magnitude more accurate than these limits, but the TAIR result barely meets them.) Figure 7 demonstrates the improvement produced by the spectral multigrid scheme over the spectral single-grid method (AFSP). There is well over an order-of-magnitude gain in efficiency.

V. A MIXED EQUATION

The potential flow problem is much more difficult whenever the flow field contains both supersonic (hyperbolic) and subsonic (elliptic) regions. Nevertheless, the spectral multigrid algorithm that succeeded for the subsonic flow case requires only a minor modification in order to succeed for the transonic (mixed) problem as well.

The most expedient technique for dealing with the mixed elliptic-hyperbolic nature of the transonic problem is to use the artificial density approach of Hafez, et al. [42]. The original artificial density is

$$\tilde{\rho} = \rho - \mu \overleftarrow{\delta \rho} \tag{99}$$

with

$$\mu = \max\left\{0, 1 - \frac{1}{M^2}\right\}, \tag{100}$$

where M is the local Mach number and $\overleftarrow{\delta}\rho$ is an upwind first-order (undivided) difference. The spectral calculations employed a higher-order artificial density formula. The spectral method also required a weak filtering technique to deal with some high-frequency oscillations generated by the shock. Details are available in [38].

Flow Past an Airfoil

A lifting transonic case is provided by the NACA 0012 airfoil at $M_\infty = 0.75$ and 2^o angle of attack. A shock appears only on the upper surface for these conditions and is rather strong for a potential calculation; the normal Mach number ahead of the shock is about 1.36. Lifting transonic cases are especially difficult for spectral methods since the solution will always have significant content in the entire frequency spectrum: the shock populates the highest frequencies of the grid and the lift is predominantly on the scale of the entire domain. An iterative scheme therefore must be able to damp error components across the spectrum.

Surface pressure distributions from MGAFSP, TAIR, and FL036 are shown in Fig. 8. The respective computational grids are 18×64, 30×149, and 32×192. The latter two are the default grids for the production finite difference codes. Spectral results obtained by trigonometrically interpolating the 18×64 grid results onto a much finer grid are included alongside the results at the collocation points. This reveals the wealth of detail that is provided by the rather coarse spectral grid. The shock predicted by TAIR is far more rounded and smeared than that of FL036, reflecting the coarser mesh and larger artificial viscosity used in the

former. The TAIR result shown is also only correct to one decimal place in lift as compared with a finer-grid result. Convergence histories for these three cases are shown in Fig. 9 along with the results for MGAFSP on a coarser grid (16 × 48).

Flow Past a Circular Cylinder

The MGAFSP code has recently been used by us for an extremely accurate determination of the critical freestream Mach number at which the potential flow past a circular cylinder first develops a supersonic region. This spectral calculation represents an alternative to the asymptotic series method employed by van Dyke and Guttmann [43] to arrive at the estimate

$M_{crit} = .39823780 \pm .00000001$.

The spectral multigrid potential code was used to determine the critical Mach number on several grids. On each of these grids calculations were performed at a half-dozen or so freestream Mach numbers. For each case the maximum local Mach number was determined from the computed solution. Then an extrapolation procedure was employed to ascertain what freestream Mach number produced a maximum local Mach number of unity. This value was recorded as the critical Mach number for that particular grid. An estimate of the extrapolation error was made to ensure consistency. These results are given in Table XI.

Finally, these grid-dependent calculations of the critical freestream Mach number were extrapolated to the limit of infinite numerical resolution. The best result was obtained by assuming sixth-order convergence. The final estimate of the critical freestream Mach number is

$M_{crit} = .3982415 \pm .0000002$. The difference between this estimate and the one by van Dyke and Guttmann is more than an order-of-magnitude greater than the

estimated errors. Nevertheless, the agreement of the two estimates to better than one part in 10^5 is remarkable in itself.

Note that the convergence rate of the spectral multigrid potential result (at least sixth-order) pertains to a quantity (critical freestream Mach number) which requires the fundamental solution (the potential) to be first differentiated and then extrapolated. Moreover, the MGAFSP code is so efficient that all of the requisite calculations consumed less than 20 minutes of CPU time on the CDC Cyber 175 and were performed on grids with no more than 2000 points.

A comparable calculation by existing finite difference codes would likely exhibit only first-order convergence. It would be far more expensive both in terms of CPU time and storage, surely exceeding the central memory of a machine such as the CDC Cyber 175. Here then is an example which firmly establishes the utility of spectral methods for nonlinear, multi-dimensional problems.

Table XI. Grid-dependent Critical Freestream Mach Numbers

Grid	M_{crit}	Error Estimate
14 × 32	.398289	.000048
18 × 40	.3982514	.0000099
22 × 48	.3982450	.0000035
30 × 64	.3982422	.0000007

References

[1] Finlayson, B. A. and Scriven, L. E., "The Method of Weighted Residuals - A Review," Appl. Mech. Rev., Vol. 19, 1966, pp. 735-748.

[2] Slater, J. C., "Electronic Energy Bands in Metal," Phys. Rev., Vol. 45, 1934, pp. 794-801.

[3] Barta, J., "Über die Naherungsweise Lösung einiger Zweidimensionaler Elastizitätsaufgaben ," Z. Angew. Math. Mech. (ZAMP), Vol. 17, 1937, pp. 184-185.

[4] Frazer, R. A, Jones, W. P., and Skan, S. W., "Approximation to Functions and to the Solutions of Differential Equations," Great Britain Aero. Res. Council, London, Report and Memo No. 1799, 1937.

[5] Lanczos, C. L., "Trigonometric Interpolation of Empirical and Analytic Functions," J. Math. Phys., Vol. 17, 1938, pp. 123-199.

[6] Clenshaw, C. W., "The Numerical Solution of Linear Differential Equations in Chebyshev Series," Proc. Cambridge Phil. Soc., Vol. 53, 1957, pp. 134-149.

[7] Clenshaw, C. W. and Norton, H. J., "The Solution of Nonlinear Ordinary Differential Equations in Chebyshev Series," Comp. J., Vol. 6, 1963, pp. 88-92.

[8] Wright, K., "Chebyshev Collocation Methods for Ordinary Differential Equations," Comp. J., Vol. 6, 1964, pp. 358-365.

[9] Villadsen, J. V. and Stewart, W. E., "Solution of Boundary Value Problems by Orthogonal Collocation," Chem. Eng. Sci., Vol. 22, 1967, pp. 1483-1501.

[10] Kreiss, H.-O. and Oliger, J., "Comparison of Accurate Methods for the Integration of Hyperbolic Equations," Report No. 36, Department of Computer Science, Uppsala University, Sweden, 1971.

[11] Orszag, S. A., "Comparison of Pseudospectral and Spectral Approximations," Stud. Appl. Math., Vol. 51, 1972, pp. 253-259.

[12] Silberman, I., "Planetary Waves in the Atmosphere," J. Meteor., Vol. 11, 1954, pp. 27-34.

[13] Orszag, S. A., "Numerical Methods for the Simulation of Turbulence," Phys. Fluids, Supplement II, Vol. 12, 1969, pp. 250-257.

[14] Eliasen, E., Machenauer, B., and Rasmussen, E., "On a Numerical Method for Integration of the Hydrodynamical Equations with a Spectral Representation of the Horizontal Fields," Report No. 2, Department of Meteorology, Copenhagen University, Denmark, 1970.

[15] Gottlieb, D. and Orszag, S. A., Numerical Analysis of Spectral Methods: Theory and Applications, CBMS-NSF Regional Conference Series in Applied Mathematics, SIAM, 1977.

[16] Salas, M. D., Zang, T. A., and Hussaini, M. Y., "Shock-fitted Euler Solutions to Shock-Vortex Interactions," Proc. of the 8th Intl. Conf. on Numerical Methods in Fluid Dynamics, E. Krause, ed., Springer-Verlag, 1982.

[17] Hussaini, M. Y., Kopriva, D. A., Salas, M. D., and Zang, T. A., "Spectral Methods for the Euler Equations," Proceedings of the Sixth AIAA Computational Fluid Dynamics Conference, Danvers, MA, July 1983.

[18] Gottlieb, D., Lustman, L., and Orszag, S. A., "Spectral Calculations of One-Dimensional Inviscid Compressible Flows," SIAM J. Sci. Statis. Comput., Vol. 2, 1981, pp. 296-310.

[19] Zang, T. A., Hussaini, M. Y., and Bushnell, D. M., "Numerical Computations of Turbulence Amplification in Shock Wave Interactions," AIAA J., to appear.

[20] Hussaini, M. Y., Salas, M. D., and Zang, T. A., "Spectral Methods for Inviscid, Compressible Flows," Advances in Computational Transonics, W. G. Habashi, ed., Pineridge Press, Swansea, UK, 1983.

[21] Pao, S. P. and Salas, M. D., "A Numerical Study of Two-Dimensional Shock Vortex Interaction," AIAA Paper 81-1205, 1981.

[22] Ribner, H. S., "Shock-turbulence Interaction and the Generation of Noise," NACA Report 1233, 1955.

[23] Zang, T. A, Kopriva, D. A. and Hussaini, M. Y., "Pseudospectral Calculation of Shock Turbulence Interactions," Proc. of the 3rd Intl. Conf. on Numerical Methods in Laminar and Turbulent Flow, C. Taylor, ed., Pineridge Press, 1983.

[24] Orszag, S. A. and Patterson, G. S., "Numerical Simulation of Three-Dimensional Homogeneous Isotropic Turbulence," Phys. Rev. Lett., Vol. 28, 1972, pp. 76-79.

[25] Orszag, S. A. and Kells, L. C., "Transition to Turbulence in Plane Poiseuille and Plane Couette Flow," J. Fluid Mech., Vol. 96, 1980, pp. 159-205.

[26] P. Moin and J Kim, "On the Numerical Solution of Time-dependent Viscous Incompressible Fluid Flows Involving Solid Boundaries," J. Comput. Phys., Vol. 35, 1980, pp. 381-392.

[27] Kleiser, L. and Schumann, U., "Spectral Simulation of the Laminar-Turbulent Transition Process in Plane Poiseuille Flow," Proc. of ICASE Symp. on Spectral Methods, R. Voigt, ed., SIAM-CBMS, 1983.

[28] Davis, P. S. and Rabinowitz, P., Numerical Integration, Blaisdell Publishing Company, 1967.

[29] Streett, C. L., Zang, T. A., and Hussaini, M. Y., "Spectral Multigrid Methods with Applications to Transonic Potential Flow," ICASE Report No. 83-11, 1983.

[30] Lanczos, C. "Legendre versus Chebyshev Polynomials," Proc. of the Royal Irish Academy Conference on Numerical Analysis, John J. H. Milles, ed., Academic Press, 1973.

[31] Haidvogel, D. B. and Zang, T. A., "The Accurate Solution of Poisson's Equation by Expansion in Chebyshev Polynomials," J. Comput. Phys., Vol. 30, 1979, pp. 167-180.

[32] Morchoisne, Y., "Resolution of Navier-Stokes Equations by a Space-time Pseudospectral Method," La Recherche Aerospatial, Vol. 5, 1979, pp. 293-309.

[33] Orszag, S. A., "Spectral Methods for Problems in Complex Geometries," J. Comput. Phys., Vol. 37, 1980, pp. 70-92.

[34] Zang, T. A., Wong, Y. S., and Hussaini, M. Y., "Spectral Multigrid Methods for Elliptic Equations," J. Comput. Phys., Vol. 48, 1982, pp. 485-501.

[35] Zang, T. A., Wong Y. S., and Hussaini, M. Y., "Spectral Multigrid Methods for Elliptic Equations II," J. Comput. Phys., to appear.

[36] Douglas, J. and Gunn, J. E., "A General Formulation of Alternating Direction Method," Numer. Math., Vol. 6, 1964, pp. 428-453.

[37] Ballhaus, W. F., Jameson, A., and Albert, J., "Implicit Approximate Factorization Schemes for the Efficient Solution of Steady Transonic Flow Problems," AIAA J., Vol. 16, 1978, pp. 573-579.

[38] Streett, C. L., "A Spectral Method for the Solution of Transonic Potential Flow About an Arbitrary Airfoil," Proc. of the Sixth AIAA Computational Fluid Dynamics Conference, Danvers, MA, July 1983.

[39] Hackbusch, W. and Trottenberg, U., eds., Multigrid Methods, Lecture Notes in Mathematics 960, Springer-Verlag, New York, 1982.

[40] Jameson, A., "Acceleration of Transonic Potential Flow Calculations on Arbitrary Meshes by the Multiple Grid Method," AIAA Paper 79-1458, 1979.

[41] Holst, T. L., "A Fast, Conservative Algorithm for Solving the Transonic Full-Potential Equation," AIAA Paper 79-1456, 1979.

[42] Hafez, M. M., South, J. C., and Murman, E. M., "Artificial Compressibility Methods for Numerical Solution of Transonic Full Potential Equation," AIAA J., Vol. 17, 1979, pp. 838-844.

[43] van Dyke, M. D. and Guttmann, A. J., "Subsonic Potential Flow Past a Circle and the Transonic Controversy," J. Austral. Math. Soc., Ser. B24, 1983, pp. 243-261.

Figure Captions

Fig. 1 Typical shock-fitted time-dependent flow model in the physical plane.

Fig. 2 Post-shock dependence of the pressure response to a pressure wave incident at 10^{o} to a Mach 3 shock. The solid line is the linear theory prediction. The circles are the spectral solution.

Fig. 3 Dependence on incident angle of the pressure response to a 0.1% amplitude pressure wave incident on a Mach 3 shock. The solid line is the linear theory result. Circles are spectral solutions; squares are finite difference solutions.

Fig. 4. Eigenvalues of the pre-conditioned matrices for semi-implicit channel flow when the streamwise wave number $k = 5$. The grid is 32×17, the Reynolds number is 7500 and the CFL number is 0.10. Note the different scale used for the central differences pre-conditioning results.

Fig. 5. Spectral (triangles) and finite difference (solid line) surface pressures for a subcritical flow.

Fig. 6. Maximum residual versus machine time for a subsonic flow.

Fig. 7. Error in lift versus machine time for a subsonic flow from single-grid (AFSP) and multigrid (MGAFSP) spectral schemes.

Fig. 8. Surface pressures for a transonic flow.

Fig. 9. Maximum residual versus machine time for a transonic flow.

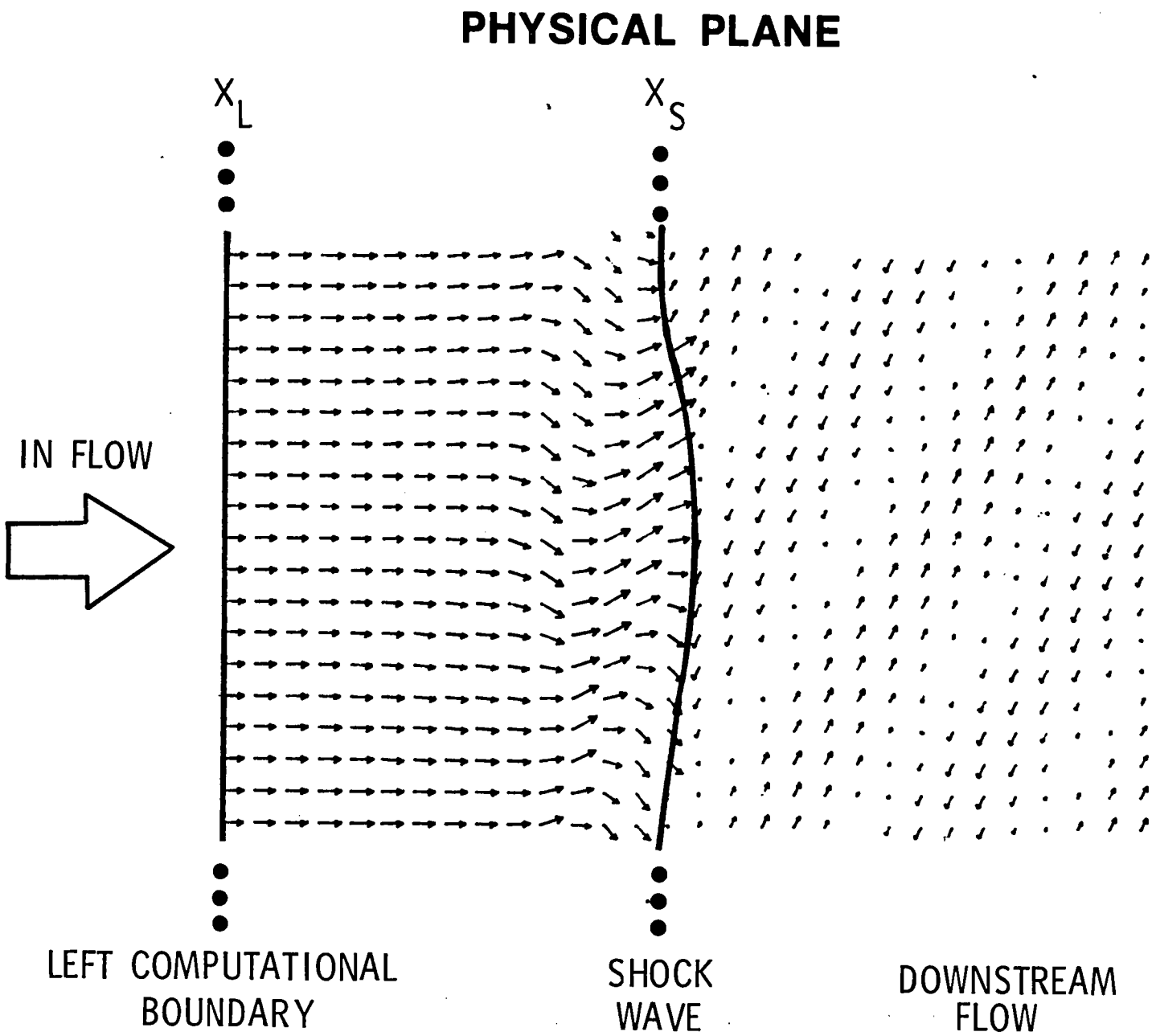
PHYSICAL PLANE
X_L
X_S
IN FLOW
LEFT COMPUTATIONAL BOUNDARY
SHOCK WAVE
DOWNSTREAM FLOW

Figure 1

ACOUSTIC RESPONSE TO 10°
INCIDENT ACOUSTIC WAVE

Mach 3

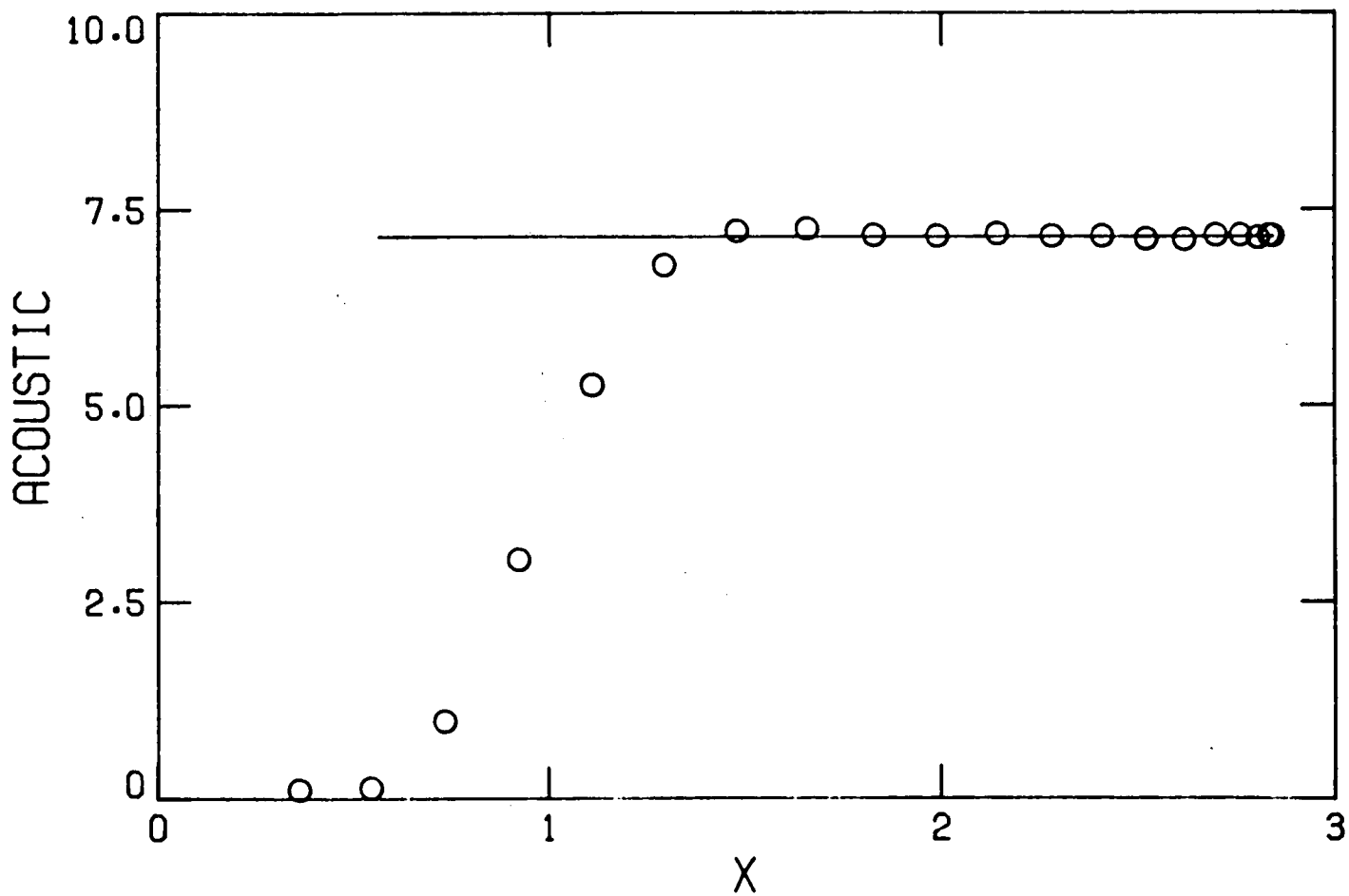

Figure 2

ACOUSTIC TRANSMISSION COEFFICIENT FOR INCIDENT ACOUSTIC WAVES

Mach 3

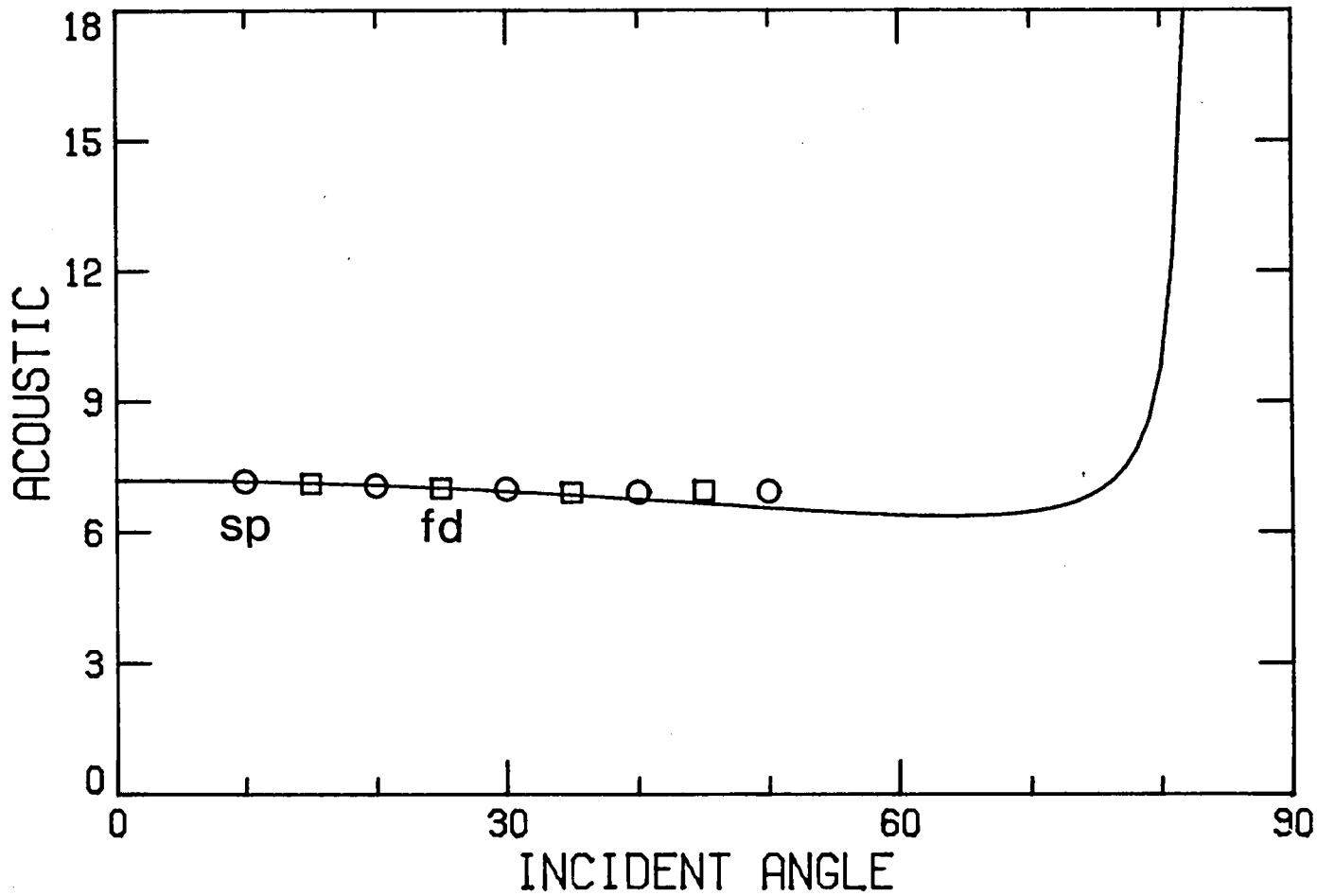

Figure 3

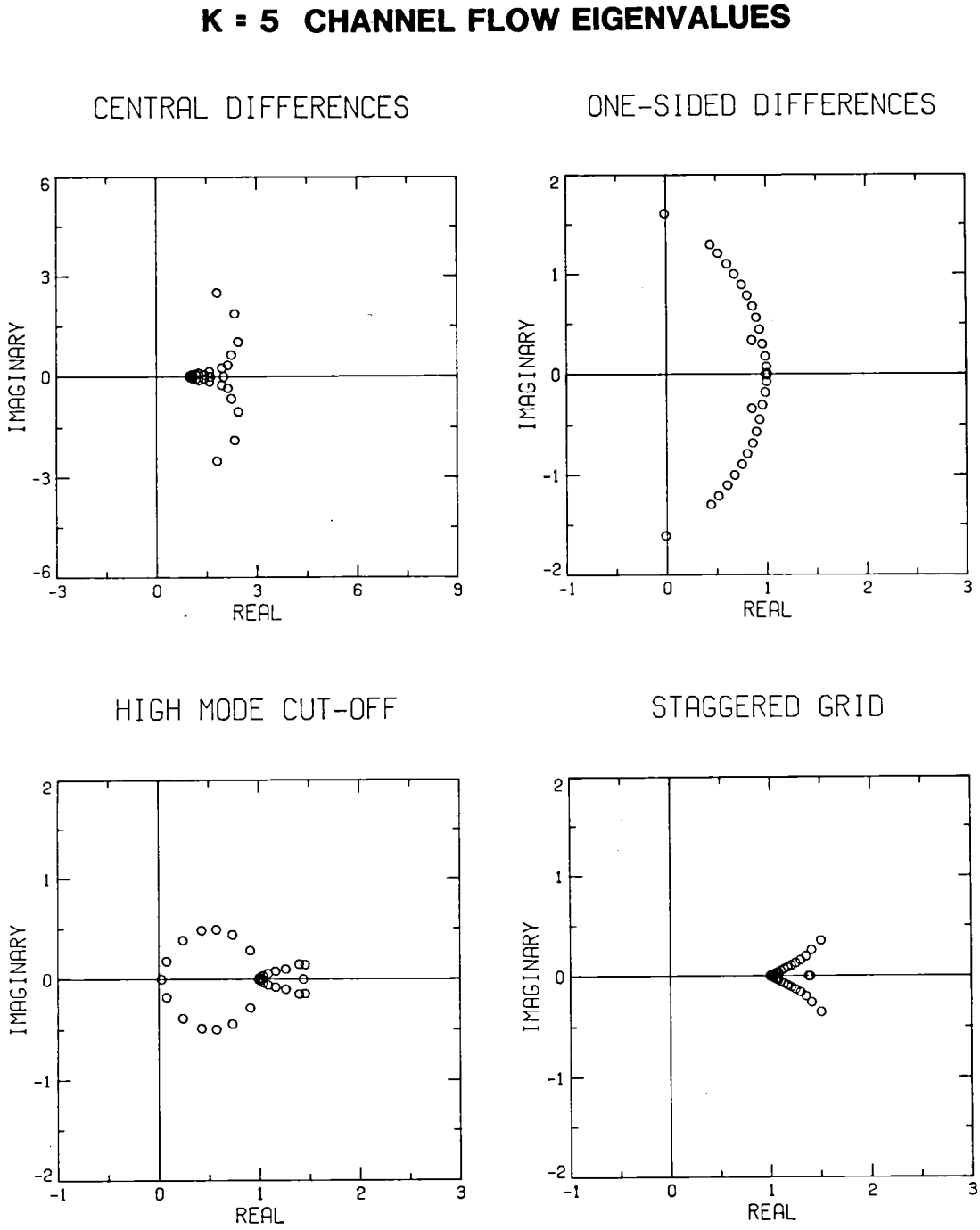
K = 5 CHANNEL FLOW EIGENVALUES
CENTRAL DIFFERENCES
ONE-SIDED DIFFERENCES
HIGH MODE CUT-OFF
STAGGERED GRID
IMAGINARY
REAL

Figure 4

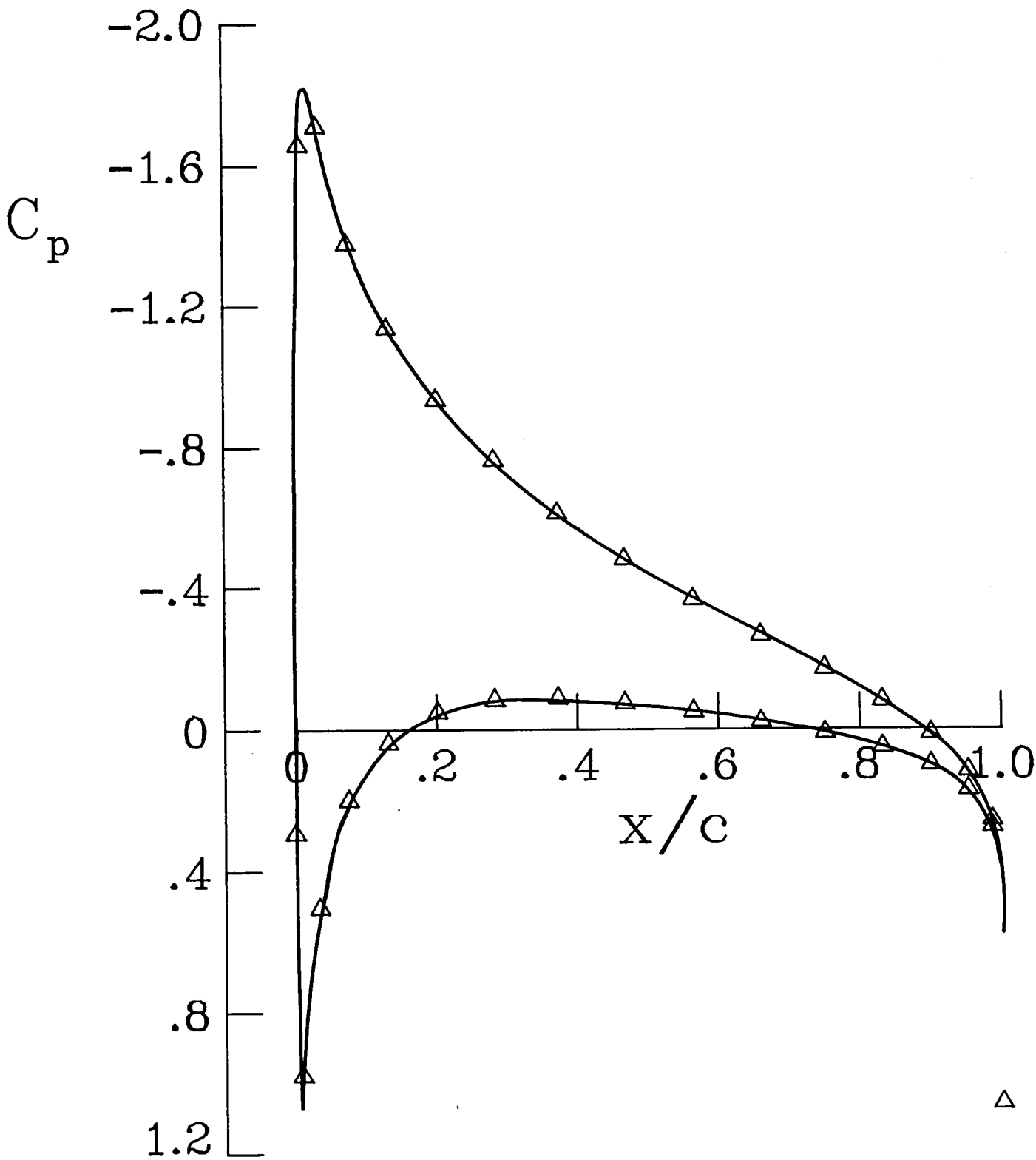

Figure 5

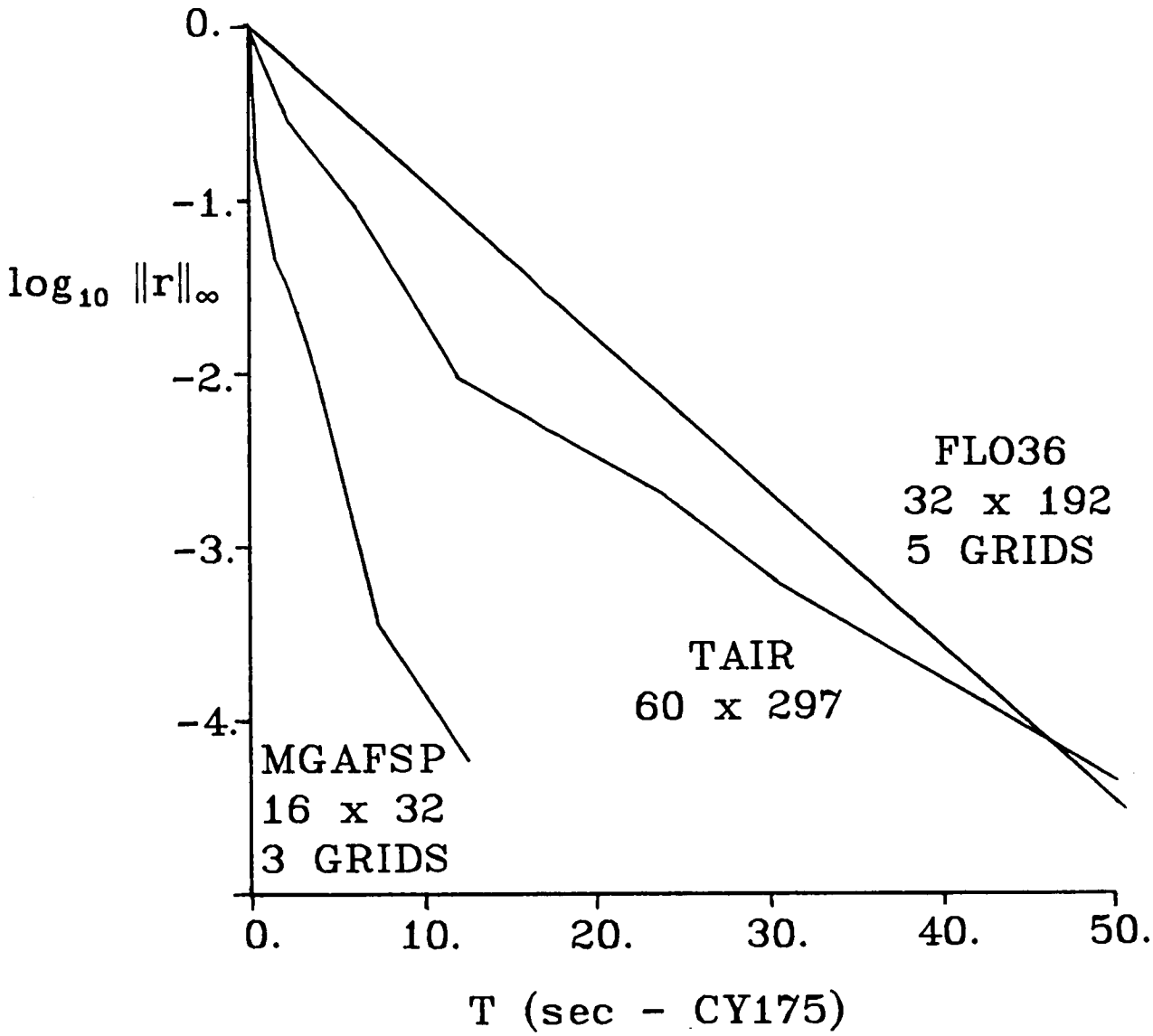
0.
-1.
-2.
-3.
-4.
log10 ||r||∞
FLO36
32 x 192
5 GRIDS
TAIR
60 x 297
MGAFSP
16 x 32
3 GRIDS
0.
10.
20.
30.
40.
50.
T (sec - CY175)

Figure 6

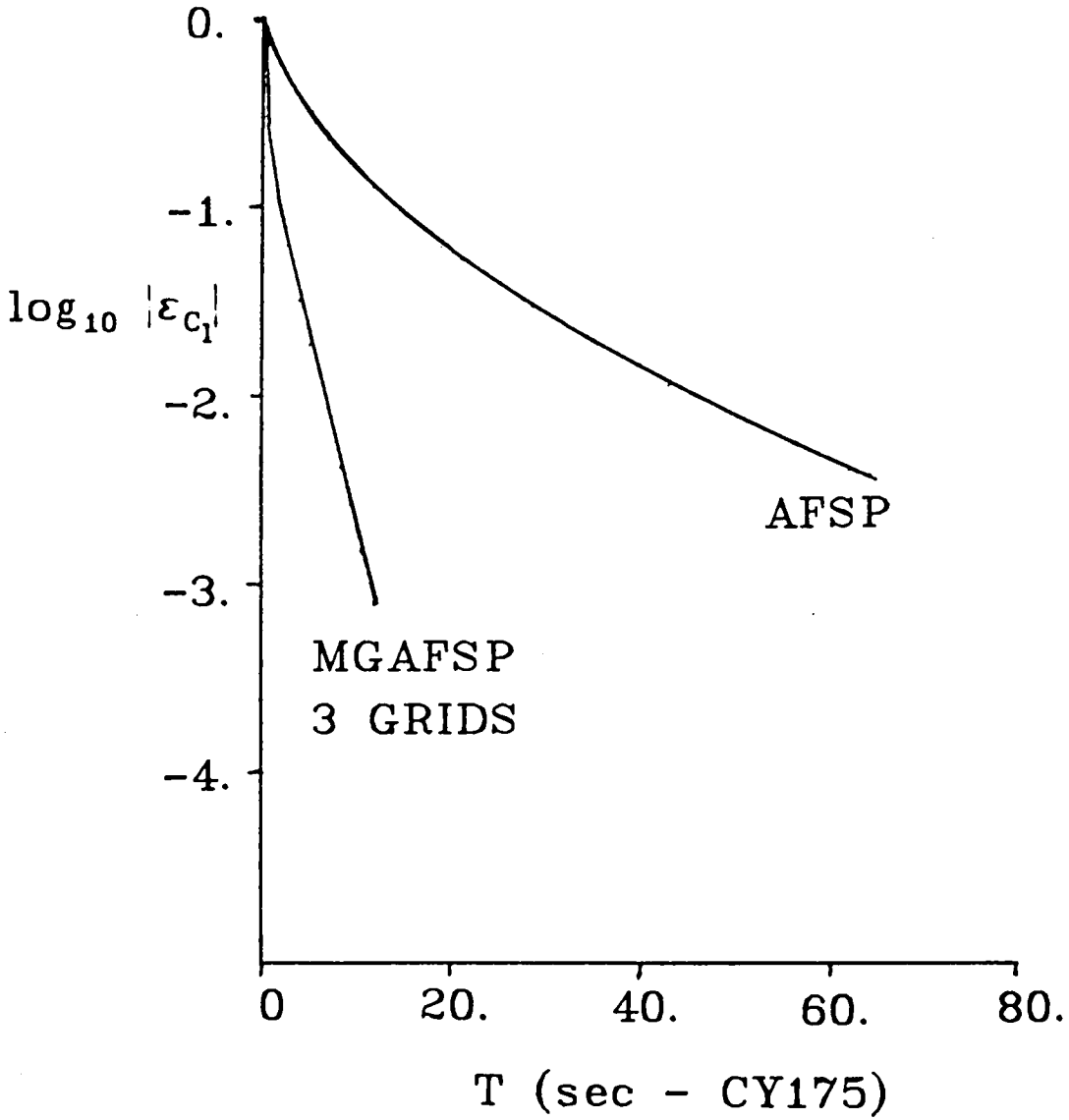

Figure 7

LIFTING, SUPERCRITICAL POTENTIAL FLOW

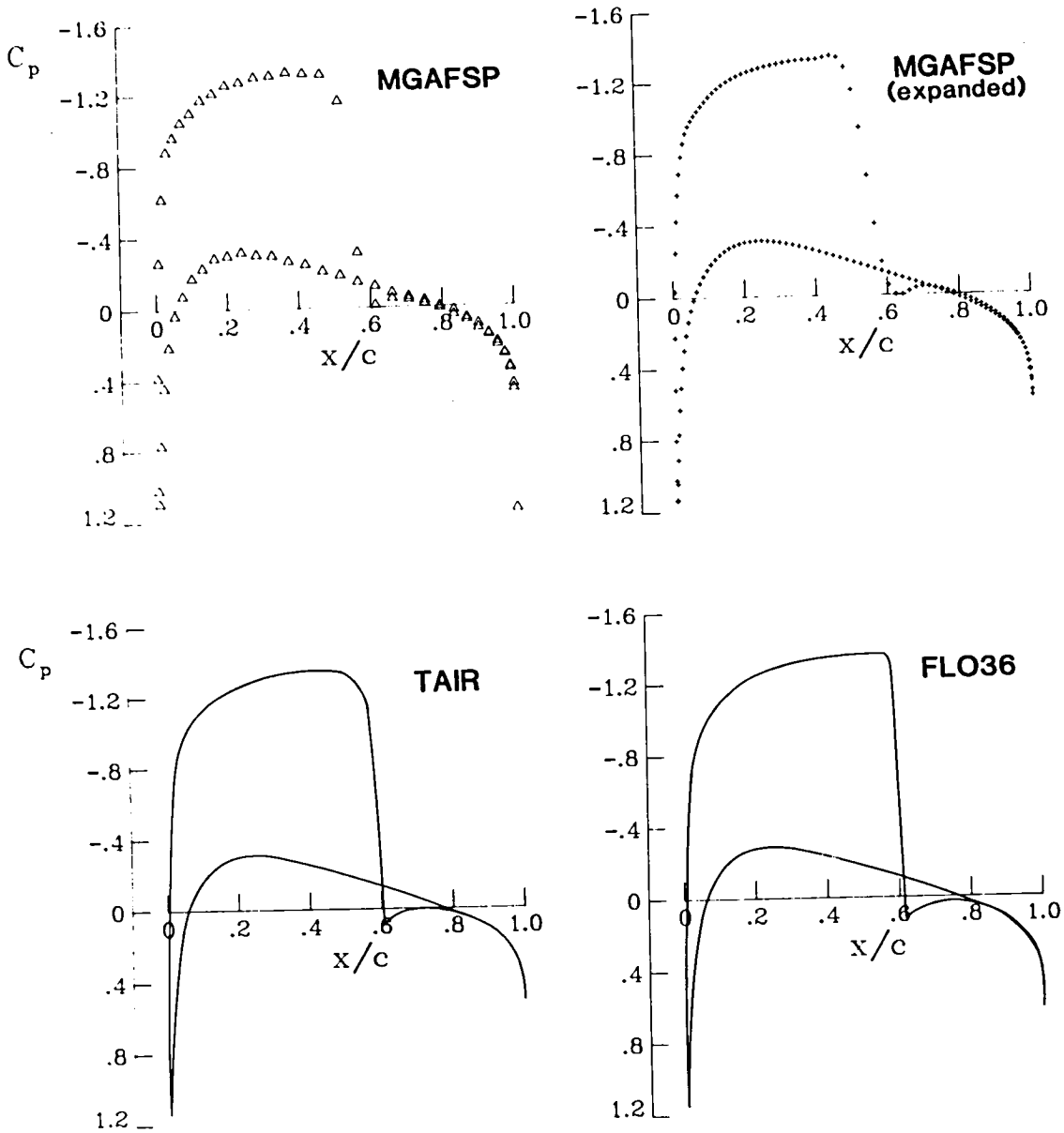

Figure 8

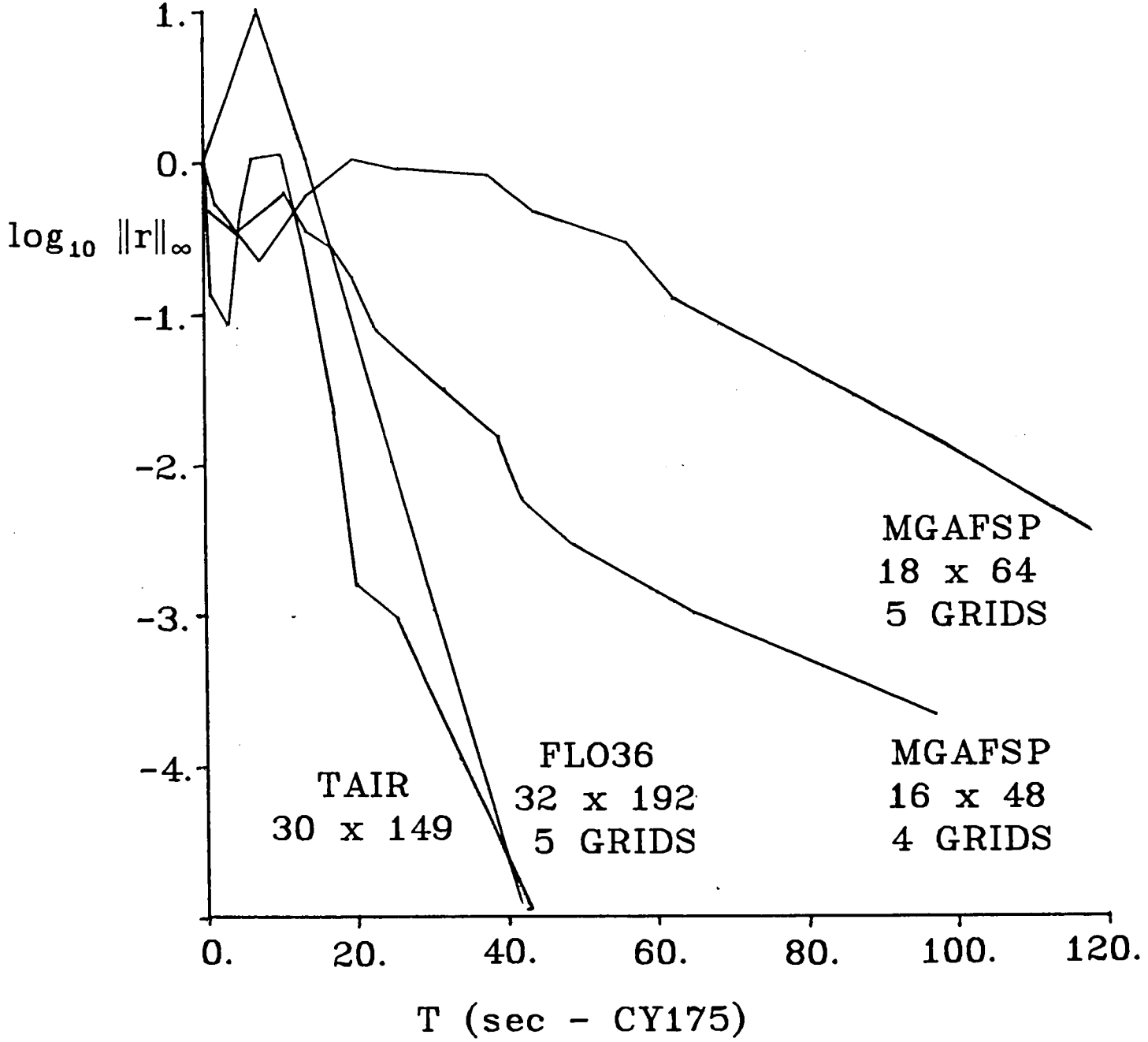
1.
0.
-1.
-2.
-3.
-4.
log10 ||r||∞
MGAFSP
18 x 64
5 GRIDS
MGAFSP
16 x 48
4 GRIDS
FLO36
32 x 192
5 GRIDS
TAIR
30 x 149
0.
20.
40.
60.
80.
100.
120.
T (sec - CY175)

Figure 9

1. Report No.	2. Government Accession No.	3. Recipient's Catalog No.
NASA CR-172248		

4. Title and Subtitle	5. Report Date
Spectral Methods for Partial Differential Equations	August 1983
	6. Performing Organization Code

7. Author(s)	8. Performing Organization Report No.
M. Yousuff Hussaini, Craig L. Streett and Thomas A. Zang	83-46
	10. Work Unit No.

9. Performing Organization Name and Address	11. Contract or Grant No.
Institute for Computer Applications in Science and Engineering Mail Stop 132C, NASA Langley Research Center Hampton, VA 23665	NAS1-17070, NAS1-17130
	13. Type of Report and Period Covered contractor report

12. Sponsoring Agency Name and Address	14. Sponsoring Agency Code
National Aeronautics and Space Administration Washington, D.C. 20546	

15. Supplementary Notes

Langley Technical Monitor: Robert H. Tolson
Final Report

16. Abstract

Origins of spectral methods, especially their relation to the Method of Weighted Residuals, are surveyed. Basic Fourier, Chebyshev, and Legendre spectral concepts are reviewed, and demonstrated through application to simple model problems. Both collocation and tau methods are considered. These techniques are then applied to a number of difficult, nonlinear problems of hyperbolic, parabolic, elliptic, and mixed type. Fluid-dynamical applications are emphasized.

17. Key Words (Suggested by Author(s))	18. Distribution Statement
Chebyshev, Legendre spectral methods elliptic, hyperbolic, parabolic and mixed equations	64 Numerical Analysis 34 Fluid Mechanics and Heat Transfer Unlimited-Unclassified

19. Security Classif. (of this report)	20. Security Classif. (of this page)	21. No. of Pages	22. Price
Unclassified	Unclassified	63	A04

For sale by the National Technical Information Service, Springfield, Virginia 22161